Markedly different impacts of primary emissions and secondary aerosol ~~formations~~formation on aerosol mixing states revealed by simultaneous measurements of CCNC, V/HTDMA, and SP2

Jiangchuan Tao[1,8], Biao Luo[1,8], Weiqi Xu[3], Gang Zhao[6], Hanbin Xu[5], Biao Xue[1,8], Miaomiao Zhai[1,8], Wanyun Xu[4], Huarong Zhao[7], Sanxue Ren[7], Guangsheng Zhou[7], Li Liu[2,*], Ye Kuang[1,8,*] , Yele Sun[3]

[1] Institute for Environmental and Climate Research, Jinan University, Guangzhou, Guangdong, China

[2] Key Laboratory of Regional Numerical Weather Prediction, Institute of Tropical and Marine Meteorology, China Meteorological Administration, Guangzhou, China.

[3] State Key Laboratory of Atmospheric Boundary Layer Physics and Atmospheric Chemistry, Institute of Atmospheric Physics, Chinese Academy of Sciences, Beijing, China.

[4] State Key Laboratory of Severe Weather, Key Laboratory for Atmospheric Chemistry, Institute of Atmospheric Composition, Chinese Academy of Meteorological Sciences, Beijing, China

[5] Experimental Teaching Center, Sun Yat-Sen University, Guangzhou, China

[6] State Key Joint Laboratory of Environmental Simulation and Pollution Control, International Joint Laboratory for Regional Pollution Control, Ministry of Education, College of Environmental Sciences and Engineering, Peking University, Beijing 100871, China

[7] Hebei Gucheng Agricultural Meteorology National Observation and Research Station, Chinese Academy of Meteorological Sciences, Beijing, 100081, China

[8] Guangdong-Hongkong-Macau Joint Laboratory of Collaborative Innovation for Environmental Quality, Jinan University, Guangzhou, Guangdong, China

Correspondence: Ye Kuang (kuangye@jnu.edu.cn), Li Liu (liul@gd121.cn)

Abstract

The aerosol mixing state is a crucial ~~physical-chemical~~physicochemical property that affects ~~their~~the optical properties and cloud condensation nuclei (CCN) activity. Multiple techniques are commonly employed to determine the aerosol mixing states for various applications, and comparisons between these techniques provide insights ~~of~~into the variations in aerosol chemical and physical properties. These techniques include size-resolved CCN activity measurements using a system with a CCN counter (CCNC) coupled with a differential mobility analyzer (DMA), a Humidified/Volatility Tandem ~~differential mobility analyzer~~Differential Mobility Analyzer (H/V-TDMA) ~~which~~that measures aerosol hygroscopicity~~/~~ and volatility distributions, and a single~~-~~particle soot photometer (SP2) ~~which~~that directly quantifies black carbon (BC) mixing states. This study provides ~~a~~the first ~~time intercomparisons~~comparison of aerosol mixing state parameters obtained through simultaneous measurements ~~of a~~using DMA-CCNC, ~~a~~ H/VTDMA, and ~~a~~ DMA-SP2. The ~~impact~~impacts of primary ~~aerosols~~aerosol emissions and secondary aerosol ~~formations~~(SA) formation on the aerosol mixing states and the intercomparison results were analyzed. The results showed that the differences in the mixing~~-~~state parameters measured ~~by~~using different techniques varied ~~greatly~~significantly under different conditions. The V-TDMA and DMA-SP2 measurements showed that the non-volatile population identified by ~~the~~ V-TDMA was mainly contributed by the BC-containing aerosols. ~~The~~ HTDMA and DMA-SP2 measurements indicated that a substantial proportion of nearly hydrophobic aerosols ~~were~~did not ~~contributed~~originate from BC-containing aerosols~~,~~ but likely originated from fossil fuel combustion and biomass~~-~~burning emissions. ~~Synthesized~~The synthesized comparison results between the DMA-CCNC, HTDMA, and DMA-SP2 measurements revealed that some ~~of the~~ nearly hydrophobic BC-free particles were CCN-inactive under supersaturated conditions, likely from fossil fuel combustion emissions~~, while~~. In contrast, others were CCN-active under supersaturated conditions linked to biomass~~-~~burning emissions. ~~Fossil fuel combustion emitted~~ BC-containing aerosols ~~tended~~emitted from fossil fuel combustion tend to be more externally mixed with other aerosol ~~compositions compared to~~components than those emitted ~~from~~by biomass~~-~~burning activities. These results highlight significant disparities in the mixing states ~~as well as~~and physiochemical properties ~~between aerosol originated~~ of aerosols from fossil fuel ~~combustion~~ and biomass burning. The formation of secondary nitrate and organic aerosols ~~exerted significant impacts on~~significantly

affects variations in aerosol mixing states, generally enhancing aerosol hygroscopicity and volatility~~,~~ while reducing differences in mixing state parameters derived from different techniques, ~~resulting in a reduction in~~reducing aerosol heterogeneity. ~~The variations in~~Variations in the number of BC-free particle ~~number~~ fractions showed that ~~secondary aerosols~~SAs tended to form more quickly on BC-free particles than on BC-containing particles. Further comparison of the mixing state parameters revealed that the two resolved ~~SOA~~secondary organic aerosol factors in this study exhibited remarkably different physical properties, indicating that they ~~were~~ likely formed through different pathways. These findings suggest that ~~intercomparisons~~comparisons among aerosol mixing states derived from different techniques can provide deeper ~~insight~~insights into ~~aerosol~~the physical properties of aerosols and how they are ~~impacted~~affected by ~~secondary aerosol~~SA formation, aiding the investigation of ~~secondary aerosol~~SA formation pathways.

1 Introduction

The aerosol mixing state is a crucial physicochemical property of aerosol particles (Riemer et al., 2019), exerting a significant impact on their optical properties and cloud condensation nuclei (CCN) activity, thus affecting their impact on the climate and ~~the~~ environment (Fierce et al., 2017; Riemer et al., 2019; Stevens et al., 2022). For ~~instance~~example, variations in the mixing state of black carbon (BC) particles can significantly alter their absorption and radiative effects (Bond et al., 2013; Lack et al., 2012; Zhao et al., 2019; Moffet et al., 2016; Matsui et al., 2018; Peng et al., 2016). Using simple ~~internally~~internal mixing state assumptions for aerosol chemical compositions ~~in estimating~~to estimate CCN number concentrations can lead to substantial overestimations (up to 30%; Deng et al., 2013; Farmer et al., 2015; Ren et al., 2018; Ching et al., 2017, 2019; Tao et al., 2021). The aerosol mixing state varies widely due to complex emissions and atmospheric transformations, leading to significant uncertainties in estimating the effects of ~~aerosol~~aerosols based on simplified mixing state assumptions (Ervens, 2015; Wang et al., 2022; Fu et al., 2022).

The aerosol mixing state describes the mixture of aerosol chemical components within each ~~single~~ particle and the distribution of these particles in the aerosol population. This property can be directly measured ~~by the~~using single-~~-~~particle chemical composition techniques (Fierce et al., 2017; Riemer et al., 2019), such as the single-~~-~~particle soot photometer (SP2~~) that~~), which measures refractory black carbon (rBC) mass concentrations and the mixing state of rBC with other aerosol components, or single-particle chemical composition measurement techniques (e.g~~.~~., single-particle aerosol mass spectrometer, SP-AMS) that have been developed ~~over~~in recent years (Lee et al., 2019; Riemer et al., 2019 and reference therein). Alternatively, the aerosol mixing state can be inferred from indirect measurements of aerosol properties, such as size-resolved aerosol CCN activity (measured by coupling a differential mobility analyzer (DMA) and a CCN counter (CCNC)), size-resolved aerosol hygroscopicity distributions, or volatility distributions (measured by a Humidified/Volatility Tandem differential mobility analyzer (H/V-TDMA)).

However, each technique yields information on aerosol mixing states based on different aerosol ~~micro-physical~~microphysical properties, thus ~~obtain~~obtaining aerosol mixing states that are different but linked to one another. For instance, while both CCN activity and ~~the~~ hygroscopic growth measurements are associated with aerosol hygroscopicity, an intercomparison between CCNC and

HTDMA measurements ~~promoted~~has prompted investigations ~~on~~into aerosol hygroscopicity variations under different saturation conditions (Su et al., 2010; Juranyi et al., 2013; Lance et al., 2013; Kawana et al., 2016; Tao et al., 2020; Jiang et al., 2021). Although ~~both~~the SP2 and VTDMA techniques depend on the evaporation of non-refractory compositions, only ~~the~~ rBC remains in the SP2 measurements~~, whereas the~~ . In contrast, non-refractory composition ~~evaporations depend~~evaporation depends on ~~thermodenuder~~the thermodynamic temperature in the VTDMA measurements. Thus, measurements of an SP2 are highly correlated to those of a VTDMA at high temperatures~~,~~ (200 °C–300 °C), with their differences reflecting variations in aerosol density, shape, or volatility (Philippin et al., 2004; Wehner et al., 2009; Adachi et al., 2018, 2019; Wang et al., 2022). HTDMA and VTDMA can be ~~applied in combination~~combined to study the influence of the aerosol mixing state on ~~its~~ hygroscopicity and volatility (Zhang et al., 2016; Cai et al., 2017; Wang et al., 2017). Strong correlations were found between the hydrophobic and non-volatile particles, suggesting ~~that~~ they might ~~be of~~have similar chemical ~~composition~~compositions (Zhang et al., 2016). In addition, some studies ~~showed~~have shown that, except for BC, low-volatility particles ~~correlated~~correlate well with CCN-inactive particles based on VTDMA and CCNC measurements (Kuwata et al., 2007; Kuwata and Kondo, 2008; Rose et al., 2011; Cheng et al., 2012). Therefore, intercomparisons between mixing state parameters measured by distinct techniques ~~provides not only~~provide a better characterization of the aerosol mixing state ~~itself, but also~~and insight into aerosol physiochemical properties. Previous studies have mainly compared two ~~kinds~~types of aerosol mixing state measurements~~, lacking~~ and lacked a comprehensive comparative analysis among SP2, DMA-CCN, and HV-TDMA measurements, hindering the wide ~~applications~~application of derived aerosol mixing states obtained by individual techniques.

The mixing state of primary aerosols can vary greatly depending on their type and emission conditions (Cheng et al~~.~~., 2012; Wang et al~~.~~., 2017; Wang et al., 2022; Ting et al., 2018; Liu et al., 2021~~),~~) and can be significantly altered during aging processes or secondary formations (Wehner et al~~.~~., 2009; Cheng et al~~.~~., 2012; Wang et al., 2022; Tomlin et al., 2021; Lata et al., 2021). Primary aerosol emissions, such as biomass burning, fossil fuel combustion, and cooking, tend to contribute to ~~weakly hygroscopic~~weak hygroscopicity (Herich et al., 2008, 2009; Wang et al., 2020; Kim et al., 2020) and low-volatility aerosols (Hong et al., 2017; Saha et al., 2018~~), while~~). The formation of

secondary ~~aerosol~~aerosols (SAs), including the aging of BC-containing aerosols and primary organic aerosols, mainly ~~contribute~~contributes to aerosols with strong CCN activity (Mei et al., 2013; Ma et al., 2016; Tao et al., 2021) and high hygroscopicity (Chen et al., 2018; Kim et al., 2020; Wang et al., 2020). ~~To enhance our understanding of the mixing state of aerosols from different emission sources and to improve its characterization in models, it~~It is important to study the impact of specific primary aerosol emissions and ~~secondary aerosol formations~~ SA formation on aerosol mixing states and the influence ~~on~~of aerosol mixing state parameters derived from different techniques to enhance our understanding of the mixing state of aerosols from different emission sources and improve their characterization in models.

The North China Plain (NCP) is among the most polluted regions in China, with various primary emission sources and strong ~~secondary aerosol~~SA formations ~~playing~~that play critical roles in air pollution (Xu et al., 2011; Tao et al., 2012; Liu et al., 2015). The complex mixing state of aerosols in the NCP contributes to uncertainties in evaluating their climate and environmental effects (Zhuang et al., 2013; Nordmann et al., 2014; Zhang et al., 2016; Tao et al., 2020; Shi et al., 2022), particularly ~~with regards to~~regarding BC particles (Wu et al., 2017; Liu et al., 2019; Zhao et al., 2019; Wang et al., 2011; Zheng et al., 2019). Meteorological conditions can greatly ~~impact the secondary aerosol~~ affect SA formation in the NCP~~, which~~ and can be significantly exacerbated during severe pollution events. SA formation under low relative humidity (RH) conditions, mainly through the condensation of gaseous-phase oxidation products, would change to that mainly occurring in the aqueous phase under high RH conditions (Kuang et al., 2020~~), and consequently~~). Because SAs formed through different mechanisms, have different chemical compositions and add mass to different aerosol populations, SA formation under different meteorological conditions can affect the aerosol mixing states ~~(Tao et al., 2021).~~differently (Tao et al., 2021). This study obtained the aerosol mixing state through concurrent measurements of the CCN activity, hygroscopicity, volatility, and BC ~~particle~~particles at a regional site in the NCP~~,~~ using CCNC, HTDMA, VTDMA, and SP2 instruments. This provides a unique opportunity to perform a ~~most~~ comprehensive ~~intercomparison~~inter-comparison of the aerosol mixing ~~state~~states among different techniques ~~for insights~~to gain insight into the impact of primary aerosol emissions and ~~secondary aerosol formations~~SA formation on the observed aerosol mixing states.

2 Materials and methods

2.1 Campaign information and instruments ~~set-up~~setup

From the 16th of October to the 16th of November 2021, aerosol mixing states were continuously and concurrently monitored using different techniques at the Gucheng site in Dingxing ~~county~~County, Hebei ~~province~~Province, China, as part of ~~the~~a campaign ~~of investigating~~to investigate AQueous Secondary ~~aerOsol formations~~aerosol formation in ~~Fogs~~fog and ~~Aerosols~~aerosols and their ~~Radiative~~radiative effects in the NCP (AQ-SOFAR). The observation site, located at 39°09'N, 115°44'E, is an Ecological and Agricultural Meteorology Station of the Chinese Academy of Meteorological Sciences, situated between the megacities of Beijing (approximately 100 km away) and Baoding (approximately 40 km away~~),)~~ and surrounded by farmlands and small towns. This site provides a representative view of the background ~~conditions of~~ atmospheric pollution conditions in the NCP (Kuang et al., 2020; Li et al., 2021).

Different measurement techniques were used ~~during the campaign~~ to simultaneously obtain the aerosol mixing state through CCN activity, hygroscopicity, volatility, and BC particle observations ~~(to be discussed in the next section).~~. In addition to aerosol mixing state measurements, the AQ-SOFAR campaign ~~also included~~includes measurements of aerosol number size distribution, chemical composition, aerosol scattering, and absorption properties. Aerosol number size distributions in the diameter range of 13 nm–4 µm were measured by the scanning mobility particle sizer (13–550 nm) and the aerodynamic aerosol classifier (100 nm–4 µm), and they are merged by assuming an aerosol density of 1.6 g/cm^3. The total ~~rBC~~BC mass concentrations were determined using an aethalometer (Magee, AE33; Drinovec et al., 2015~~), with~~); more information ~~about~~on the correction of ~~the~~ absorption measurements and mass concentration calculations is available in Luo et al. (2022). All aerosol measurement instruments were housed in a temperature-controlled container ~~set at 24 °C.~~ at 24 °C. The inlet was switched among three impactors: TSP (Total Suspended Particles), $PM_{2.5}$ (Particulate Matter with an aerodynamic diameter of less than 2.5 µm), and PM_1 (Particulate Matter with an aerodynamic diameter of less than 1 µm). Inlet changes among impactors affect dry-state aerosol sampling owing to ambient aerosols are enlarged through aerosol hygroscopic growth or activation. However, the aerosol mixing state and aerosol chemical composition measurements were made on submicron aerosols, and the inlet change almost did not affect those measurements under

conditions of RH less than 90%. The sampled aerosol was dried by two parallelly assembled Nafion dryers with a length of 1.2 m. Two Nafion driers was used because of the high RH and sample flow rate (~16 L/min) during the campaign to ensure drying efficiency. In addition, during autumn and winter in the NCP, ambient air temperature (<20 °C and sometimes <0 °C) can be significantly lower than the room temperature (~24 °C). Therefore, this dryer system can maintain the RH of sampled aerosols to below 20%. Meteorological data~~,~~ such as temperature, pressure, wind speed ~~and~~, wind direction, ~~relative humidity (RH),~~and RH were obtained from an automatic weather station operated by the station.

The chemical composition of the submicron aerosols was analyzed using a High-Resolution Time-of-Flight Aerosol Mass Spectrometer (HR-ToF-AMS). The ionization efficiency (IE) was calibrated using 300 nm diameter pure NH_4NO_3 particles, following the standard protocols outlined in Jayne et al. (2000) in the middle of the campaign, with the relative ionization efficiency (RIE) of ammonium determined to be 5.26. The RIE of sulfate was 1.28 using pure $(NH_4)_2SO_4$ particles, and the default RIEs of 1.4 for organic aerosols, 1.1 for nitrates, and 1.3 for chlorides were used~~.~~ as the organic aerosols. The composition~~-~~dependent collection efficiency reported by Middlebrook et al. (2012) was used ~~in this study~~. Elemental ratios were derived using the "Improved-Ambient (I-A)" method as described in Canagaratna et al. (2015), including hydrogen to carbon (H/C), oxygen to carbon (O/C), and organic mass to organic carbon (OM/OC) ratios. Two primary organic aerosol (POA ~~factors~~) and two ~~SOA~~oxygenated organic aerosol (OOA) factors were identified by High-Resolution Positive Matrix Factorization (HR-PMF ~~(~~; Ulbrich et al., 2009; Paatero and Tapper, 1994). This study used the summation of the two OOA factors to represent secondary organic aerosols (SOA). The mass spectra of the organic aerosol (OA) factors and their correlations with external species are shown in Figs. S1~~-~~ and S2. The Biomass Burning Organic Aerosol (BBOA) spectrum was characterized by obvious *m*/*z* 60 (mainly $C_2H_4O_2^+$) and 73 (mainly $C_3H_5O_2^+$), two indicators of biomass burning (Mohr et al., 2009). ~~In addition,~~ BBOA ~~was~~ correlated well with $C_2H_4O_2^+$ (R^2=0.91) and $C_3H_5O_2^+$ (R^2=0.90). Consistent with previous studies in Beijing (Xu et al., 2019), the PMF analysis revealed a mixed factor named Fossil Fuel Organic Aerosol (FFOA ~~that~~), which comprises traffic emissions and coal ~~combustions, which was~~combustion and is characterized by a typical hydrocarbon ion series. ~~It was observed that~~ FFOA had a relatively high f_{44} (0.083) value, which ~~is~~was likely due to aging during regional transportation, similar to the results observed in the winter of 2016 in Beijing (Xu et al., 2019)

and ~~CCOA~~coal combustion organic aerosols in Gucheng (Chen et al., 2022). ~~Two SOA~~Secondary organic aerosol formation from volatile organic compound precursors could occur in different formation pathways, such as aqueous-phase, heterogeneous, or gas-phase reactions. It might also be oxidized under different conditions, such as oxidation under different nitrogen oxide conditions with different oxidation capacities and oxidants. The two resolved OOA factors ~~were found to display~~displayed different spectral patterns, correlations with tracers, and diurnal variations, suggesting that they resulted from different chemical ~~processing. For example,~~ processes. However, their formation mechanisms remain to be explored in future studies. In general, the OOA factor 1 (OOA1 ~~had~~) has higher $CO_2^+/C_2H_3O^+$ (3.9) and O/C (0.91) ratios than OOA factor 2 (OOA2) with 2.1 and 0.78, respectively.

This study did not consider losses in the inlet line and sampling systems for the following reasons: (1) investigated mixing state parameters are represented by number fractions (NFs) of different diameters, which are much less affected by losses in sampling systems compared ~~to OOA2 (2.1, 0.78~~with absolute number concentrations; and (2) good consistency was achieved between measurements of particle number size distributions (PNSD) and mass concentrations measured by AMS. The average ratio between volume concentration derived from AMS and rBC measurements (densities of compounds are the same as Kuang et al., 2021) and the volume concentration derived from PNSD measurements was 0.79 (R=0.97, as shown in Fig. S3), consistent with previous reports as AMS cannot detect aerosol components, such as dust (Kuang et al., 2021).

2.2 Aerosol mixing states measurement techniques

2.2.1 DMA-CCNC measurements

The CCN activity of the particles under supersaturated conditions was measured using a DMA-CCNC system, which consisted of a differential mobility analyzer (DMA~~,~~; model 3081 ~~by,~~ TSI, Inc., MN, USA), ~~a~~ condensation particle counter (CPC~~,~~; model 3756 ~~by,~~ TSI, Inc., MN, USA), and ~~a~~ continuous-flow CCNC (model CCN100 ~~by,~~ Droplet Measurement Technologies, USA). The system was operated in ~~a~~ size-scanning mode and provided the Size-resolved Particle Activation Ratio (SPAR) by combining ~~the~~ CPC and CCNC measurements at different particle sizes. ~~Three~~To compare the instruments, three supersaturations (SSs) of 0.08%, 0.14~~%~~%, and 0.22% were applied in a single cycle of ~~about~~approximately 15 ~~minutes.~~min. CCN measurements under these three SSs revealed that the

CCN activity of aerosols resides in the accumulation mode with an aerosol diameter range of approximately 100–200 nm, which is close to the diameters of the HV-TDMA measurements. Higher SSs would reveal CCN activities of smaller aerosol particles (<100 nm), where the DMA-SP2 measurement is unavailable. The sample and sheath flow rates of ~~the~~ DMA were set at 1 ~~lpm~~ and 5 lpm, respectively, resulting in a measured particle diameter range of 9~~ nm to~~ –500 nm, with a running time of 5 ~~minutes~~min per cycle. ~~Supersaturations~~Supersaturation in the CCNC ~~were~~was calibrated with monodisperse ammonium sulfate particles (Rose et al., 2008)~~ both~~ before and after the campaign. The flow rates were also calibrated before and after the campaign and ~~were~~ checked daily to minimize uncertainties in~~ the~~ droplet counting and supersaturation formed in the column (Roberts and Nenes, 2005; Lance et al., 2006). ~~The~~ SPAR deviations due to multiple-charge particles were corrected using a modified algorithm based on Hagen and Alofs (1983) and Deng et al. (2011). ~~More~~Further details ~~about the~~regarding this system can be found in Ma et al. (2016) and Tao et al. (2021).

2.2.2 H/V-TDMA measurements

The mixing state of the aerosols in terms of hygroscopicity and volatility was measured using a Hygroscopicity/Volatility Tandem Differential Mobility Analyzer (H/V-TDMA; Tan et al., 2013). The H/V-TDMA ~~consists~~consisted of two DMA (Model ~~3081L~~3081 L, TSI Inc.), with the first DMA (DMA1) selecting dried particles without conditioning (RH ~15%) and the second DMA (DMA2) selecting conditioned particles. ~~The~~ H/V-TDMA can operate in either H-~~mode~~ or V-mode, ~~which is~~ controlled by a three-way solenoid valve. ~~In H-mode, a~~A Nafion humidifier ~~is~~was used in the H-mode to condition the selected dry particles to 90% ~~relative humidity (RH)~~RH equilibrium. The number~~-~~-size distribution of ~~the~~ humidified particles (D_p) ~~is~~was measured ~~by~~using DMA2 and ~~a~~ CPC (Model 3772, TSI Inc.). The RH-dependent hygroscopic growth factor (GF) at a ~~certain dry~~specific diameter ~~is~~(D_d) was calculated as follows:

$$GF=\frac{\sout{D_p}}{\sout{D_d}}\frac{D_p(RH)}{D_d} \quad (1)$$

~~In this mode, four~~where $D_p(RH)$ is the size of particles undergoing humidification. Four dry electrical mobility diameters (50, 100, 150, and 200 nm) were measured~~.~~ in this mode. The instrument was regularly calibrated using ~~Standard Polystyrene Latex Spheres~~standard polystyrene latex spheres (PSL) and ~~Ammonium Sulfate~~ammonium sulfate particles.

In ~~the~~ V-mode, a heated tube ~~was used to evaporate~~evaporated the volatile coatings from the previously selected dry particles. Six temperature settings were used for the heated tube, ranging from 25 ~~to~~ 200°C. The number~~-~~size distributions of the heated particles were measured using DMA2 and CPC. ~~Besides~~ In addition to the four particle sizes measured in the H-mode, three additional particle sizes (250, 300, and 350 nm) were measured in the V-~~-~~mode~~.~~ (residence time inside the heated tube to be about 1.6 s; Hong et al., 2017). The temperature~~-~~dependent shrinkage factor (SF), which is the ratio of ~~the~~ heated particle size to ~~the~~ dry particle size~~,~~ without heating (D_d), is defined as:

$$SF=\frac{\frac{D_p}{D_d}}{\frac{D_p(T)}{D_d}} \quad (2)$$

where $D_p(T)$ denotes the particle diameter during heating. A complete cycle of ~~both~~ H-mode measurements ~~at~~under one ~~relative humidity (~~RH~~)~~ condition and V-mode measurements at six ~~temperature conditions~~temperatures took approximately 3 ~~hours. A~~h. The Probability Density Function (PDF) of the GF (or SF) ~~can be~~was calculated from the measured density function using the inversion algorithm described by Stolzenburg and McMurry (2008).

2.2.3 DMA-SP2 measurements

The size-resolved BC mixing states were measured ~~by the~~using an SP2 (Droplet Measurement Technology, Inc., USA) after ~~a~~ DMA (Model 3081, TSI, USA). The DMA selected aerosols ~~at~~of various dry particle sizes, which were then introduced ~~to the~~into SP2. The DMA-SP2 setup was able to measure the mixing states of aerosols ~~at~~with diameters (detection limit of approximately 80 nm based on the calibration) of 100 ~~nm~~, 120 ~~nm~~, 160 ~~nm~~, 200 ~~nm~~, 235 ~~nm~~, 270 ~~nm~~, 300 ~~nm~~, 335 ~~nm~~, 370 ~~nm~~, 400 ~~nm~~, 435 ~~nm~~, 470 ~~nm~~, 500 ~~nm~~, 535 ~~nm~~, 570 ~~nm~~, 600 ~~nm~~, 635 ~~nm~~, 670 ~~nm,~~, and 700 nm within 20 ~~minutes,~~min when it ~~wasn't~~was not placed after ~~a thermodenuder~~an enuder-bypass switch system~~.~~ (the 13th to the 24th of October, 09:00 am of the 5th of November to 09:00 am of the 8th of November). However, it only measured mixing states at diameters of 120 ~~nm~~, 160 ~~nm~~, 200 ~~nm~~, 250 ~~nm~~, 300 ~~nm~~, 400 ~~nm~~, and 500 nm when it was placed after a thermodenuder-bypass switch system~~.~~ (11:00 am of the 24th of October to 08:00 am of the 5th of November, and 09:00 am of the 8th of November to 06:00 pm of the 17th of November). Because the HTDMA and VTDMA measurements were conducted solely by a single H/VTDMA system operating in different modes, the time needed for a single particle size measurement of HTDMA and VTDMA was much longer than that of the DMA-

SP2 system. Thus, more particle sizes were selected in the DMA-SP2 system for acquiring the BC mass concentration and mixing state at larger diameters than HTDMA and VTDMA.

The SP2 chamber ~~has~~had a continuous Nd:~~-~~YAG laser beam ~~at~~with a wavelength of 1064 nm. The BC-containing particles passing through the laser beam ~~will be~~became incandescent ~~through~~by absorbing ~~the~~ radiation. ~~By~~The mass concentration of the BC was calculated by measuring the intensity of the emitted incandescent light~~, the mass concentration of BC can be calculated.~~. The sheath flow/sample flow ratio was maintained at 10 for the DMA to reduce the width of the diameter distribution of the selected monodisperse aerosols. Additionally, the flow rate of the SP2 was changed from 0.1 to 0.12 L/min starting on ~~October~~the 22nd~~. The~~ of October (allowed flow rate range of SP2: 0.03–0.18 L/min from the specification). SP2 was calibrated using ~~Aquadag~~quadag soot particles, as reported by Gysel et al. (2011). Further details ~~about~~regarding the calibrations are ~~introduced~~provided in Section 1 of the ~~supplement~~Supplementary Information.

2.3 Derivations of mixing state parameters

2.3.1 Fitting SPAR curves measured by the DMA-CCNC system

The ~~measured~~ SPAR curves ~~can be~~were parameterized ~~with~~using a sigmoidal function with three parameters. As shown in Fig. S4, a sigmoidal curve generally characterized the measured SPAR. This parameterization assumes that the aerosol is an external mixture of CCN-active hydrophilic ~~particles that are CCN-active~~ and CCN-inactive hydrophobic particles ~~that are CCN-inactive~~ (Rose et al., 2010). The formula used to parameterize the SPAR ($R_a(D_d)$) for a specific SS is as follows (Rose et al., 2008):

$$R_a(D_d)=\frac{MAF}{2}\left(1+\mathrm{erf}\left(\frac{D_d-D_a}{\sqrt{2}\sigma}\right)\right) \quad (7)$$

where erf ~~is~~denotes the error function. The Maximum Activation Fraction (MAF) is an asymptote of the measured SPAR curve ~~at~~for large ~~particle sizes, and it represents the number~~ particles, as shown in Fig. S4, representing the fraction of CCNs relative to the total number of particles. D_a is the midpoint activation diameter ~~and~~, is linked to the hygroscopicity of the CCNs~~.~~, and indicates the diameter where the SPAR equals half of the MAF value. The σ is the standard deviation of the cumulative Gaussian distribution function and characterizes the heterogeneity of CCN hygroscopicity. In Fig. S4, the σ indicates the slope of the steep increase in the SPAR curves when the diameter is close to Da. Generally,

hydrophilic particles larger than D_a can become CCN~~, so~~. Therefore, these three parameters can be used to characterize the hygroscopicity of ~~those~~these hydrophilic particles. This study did not consider the impact of nearly hydrophobic particles on SPAR, as deviations from this parameterization scheme due to this impact ~~are~~were negligible at low SSs, as stated in Tao et al. (2020).

2.3.2 Classification of particle type based on hygroscopicity or volatility

In this study, ambient aerosol particles were classified into two groups based on their hygroscopicity (hydrophobic and hydrophilic) and two groups based on their volatility (non-volatile and volatile) based on the measurements from H/V-TDMA (Wehner et al., 2009; Liu et al., 2011; Zhang et al., 2016). Each group can be defined using ~~a~~the critical ~~value~~values of GF or SF as ~~the following:~~ follows: hydrophobic population: $GF<GF_C$; hydrophilic population: $GF\geq GF_C$; non-volatile population: $SF\geq SF_C$; and volatile population: $SF<SF_C$.

~~Hydrophobic population: $GF < GF_C$;~~

~~Hydrophilic population: $GF \geq GF_C$;~~

~~Non-volatile population: $SF \geq SF_C$;~~

~~Volatile population: $SF < SF_C$.~~

The critical values of GF (GF_C) and SF (SF_C) in H/V-TDMA depend on the particle size and working conditions, such as relative humidity and heating temperature.

During this campaign, the SF_C was set ~~at~~to 0.85 for all seven measured particle sizes at a temperature of 200 °C. The GF_C for the four measured particle sizes of 50, 100, 150, and 200 nm were 1.1, 1.15, 1.175, and 1.2, respectively, and the corresponding hygroscopicity parameter, κ, was approximately 0.07. These values of GF_C and SF_C divide the probability density functions (PDFs) of SF and GF into two modes, consistent with prior NCP studies ~~in the NCP~~ (Liu et al., 2011; Zhang et al., 2016). The ~~number fraction (~~NF~~)~~ for the hydrophilic group (NF_H) and volatile group (NF_V) can be calculated as~~:~~ follows:

$$NF_H = \int_{GF_C}^{\infty} GFPDF(GF)dGF \quad (7)$$

$$NF_V = \int_0^{SF_C} SFPDF(SF)dSF \quad (8)$$

where GFPDF and SFPDF are the PDFs of GF and SF, respectively, derived from H/V-TDMA measurements.

2.3.3 Classification of particle type based on DMA-SP2 measurements

~~The~~ BC-containing aerosols can be categorized into two groups based on ~~the~~ coating thickness: bare BC/thinly coated BC particles and thickly coated BC particles. For the measurement of coated BC particles at SP2, the incandescence signal is generally detected later than the scattering signals and the time difference between the occurrence of the peaks of the incandescence and scattering signals is defined as the lag time (Moteki & Kondo, 2007; Sedlacek et al., 2012; Subramanian et al., 2010). The coating thickness of ~~the~~ BC-containing aerosols in the SP2 measurement can be ~~determined~~indicated by the lag time ~~between the peak of the scattering signal and the incandescence signal~~ (Moteki and Kondo, 2007; Schwarz et al., 2006; Sedlacek et al., 2012; Subramanian et al., 2010; Metcalf et al., 2012~~).~~), which has exhibited a clear two-mode distribution in previous studies (Zhang et al., 2018; Zhao et al., 2021). A critical lag~~-~~ time threshold can be used to differentiate between the different types of BC-containing aerosols and calculate the ~~number fraction~~NF of bare ~~BC particles~~ and coated BC particles in the total identified aerosols. In this study, a two-mode distribution of the lag~~-~~ time (Δt) was observed, and a critical value of 0.8 μs was used to classify the BC-containing particles into thinly coated (or bare) BC (Δt ~~<~~ ≤0.8 μs) and thickly coated BC (Δt ~~≥~~ ≥0.8 μs~~), respectively.~~). The definitions of all abbreviations are listed in Table 1.

3 Results and discussions

3.1 Campaign ~~Overview~~overview

The time series of the meteorological parameters, aerosol mixing state measurements using different techniques, and mass concentrations of the aerosol chemical compositions are shown in Fig. 1. In detail, the measurements of aerosol mixing states include SPAR at an SS of 0.08~~%,~~% by DMA-CCNC, GF-PDF (PDF of GF) at 200 nm by HTDMA, SF-PDF (PDF of SF) at 200 nm and 200 °C~~,~~ by VTDMA, and lag~~-~~ time PDF of 200 nm BC-containing particles ~~and mass concentrations of~~ by

DMA-SP2. The SIA ~~(secondary inorganic aerosol), SOA (OOA1 and OOA2), PA (BBOA and FFOA),~~ SOA, POA, and BC mass concentrations are shown in Fig. 1~~. During the campaign, three~~ (b). Three periods with significantly different aerosol pollution conditions were identified~~.~~ during the campaign. As shown in Fig. 1(b), before the 23rd of October ~~23rd~~ (moderately polluted period), the accumulation of aerosols led to SIA mass concentrations ~~greater than~~ <20 μg/m^3~~, while~~. In contrast, the highest mass concentrations of SOA, POA, and BC ~~mass all~~ reached 10 μg/m^3. The mass concentrations of different ~~chemical compositions~~aerosol components increased significantly from the 23rd of October ~~23rd~~ to the 6th of November ~~6th~~ (heavily polluted period with an average non-refractory PM_1 mass concentration of 49.5±22.5 μg/m^3) and decreased ~~to~~too much lower levels after the 6th of November ~~6th~~(clean period~~).~~ with a non-refractory PM_1 mass concentration of 5.1±3.3 μg/m^3). Two particle groups were identified ~~with regard to~~concerning the CCN activity, hygroscopicity, volatility, and coating thickness, as demonstrated by the SPAR, GF-PDF, SF-PDF, and ~~the~~ lag-time PDF of BC-containing particles. Significant variations in the aerosol mixing states were also observed during the three periods ~~of~~with different pollution conditions, as demonstrated by the variations in SF-PDF measured by ~~the~~ VTDMA. For example, the SF of the non-volatile particle group decreased during the heavily polluted period. Aerosol mixing states may have changed ~~due to~~because of various transformations ~~of~~in existing aerosol particles and distinct secondary formation processes under different pollution conditions (Kuang et al., 2020; Tao et al., 2021; Shi et al., 2022; Yang et al., 2022). ~~This will be analyzed in detail later in the discussion. The diurnal~~Diurnal variations in the mass concentrations of different aerosol chemical ~~compositions~~components and mixing states can be ~~seen~~observed in the variations ~~of~~in the SPAR measurements, as previously observed in this region (Liu et al., 2011; Ma et al., 2012; Kuang et al., 2015; Tao et al., 2020).

~~In~~ Fig. 2~~,~~ shows the campaign~~-~~averaged SPAR at the three SSs, PDF of the lag~~-~~time of BC~~-~~containing particles, GFPDF, and SFPDF at 200 °C ~~at~~for different particle sizes~~ are presented.~~. The sigmoidal SPAR curves were characterized by a rapid increase, followed by a gradual increase to unit 1, similar to the measured SPAR curves previously observed in this region (Deng et al., 2011; Zhang et al., 2014; Ma et al., 2016; Tao et al., 2018). At lower SSs, the particle size required for CCN activation was larger; thus, rapid increases in the SPAR curves ~~occur~~occurred at larger particle sizes ~~and~~. In addition, the maximum AR of the SPAR curves ~~becomes smaller.~~decreases as fewer particles

are CCN-active under low SSs. For the three measured SSs, the ~~corresponding fitting parameters, Da, which indicate the center of the particle size range with rapid increases in~~particle sizes where SPAR ~~curves,~~equals approximately 0.5 are approximately 90 ~~nm~~, 120 ~~nm,~~ and 180 ~~nm,~~ nm for the three SSs of 0.08%, 0.14%, and 0.22%, respectively~~.~~, consistent with the average D_a (see Eq. 7) values of the campaign. The ~~number fraction~~NF of CCN-active particles in large ~~-~~-diameter ranges (which varies with SS and, for example, is greater than 200 nm for 0.08%) can be indicated by the gradual increase ~~of~~in the SPAR curves and quantified by the fitting parameter, MAF~~.~~ (see Eq. 7). The PDFs of the lag~~-~~time, GF, and SF ~~are~~were all characterized by a bimodal distribution, which indicates two particle groups of BC-containing aerosols with different coating thicknesses, hygroscopicity, and volatility. The variations in the aerosol mixing ~~state will be~~states were further analyzed based on the ~~basis of MAF and the number fractions (NF) of hydrophilic particles (NF_H), volatile particles (NF_V), BC-free particles (NF_{noBC}) and number fractions of thinly coated BC in BC containing aerosols (R_{exBC}).~~measured mixing state parameters.

3.2 Intercomparisons among aerosol mixing state parameters derived using four techniques

The size~~ dependence of MAF, NF_H, NF_V (200 °C), NF_{noBC}~~-dependent characteristics of the aerosol mixing state parameters derived from the measurements of the four techniques and ~~R_{exBC}~~the MFs of different aerosol chemical compositions during the three pollution periods are shown in Fig. 3. In general, the size~~ dependence~~-dependent characteristics of MAF, NF_H, NF_V, and NF_{noBC} were similar~~ to one another~~, suggesting that they were likely dominated by the same particle group, namely BC-free particles. This particle group had the ~~lowest~~highest fraction (>0.7) during the heavily polluted period and the ~~highest~~lowest fraction (down to 0.5) during the clean period, with the fraction decreasing with increasing particle size. This suggests that primary emissions tend to have higher fractions of BC-containing particles in larger diameter ranges~~. Since~~; for example, the fraction of BC-containing particles increases from ~0.1 to ~0.4 as the particle size increases from 200 to 500 nm during the cleaning period. Because the bulk aerosol ~~mass fraction (~~MF~~)~~ is mostly contributed by particles ~~larger than~~ >300 nm, there ~~might~~may have been more hydrophilic, volatile, CCN-active, and BC-free particles ~~in~~with larger sizes (>~~-~~300 nm) during the heavily polluted period~~, due~~ owing to strong ~~secondary aerosol~~SA formation in larger diameter ranges (Kuang et al., 2020), resulting in a higher

~~number fraction~~NF of these particles compared to the clean period. As for R_{exBC}, the small size dependence of R_{exBC} during the moderately polluted period might have been associated with stronger primary emissions, while the decrease ~~of~~in R_{exBC} with increasing particle diameter ~~size~~ in the polluted period ~~confirms the~~confirmed that SA formation is more efficient ~~secondary aerosol formation in~~for particles with larger ~~diameter ranges~~diameters.

As for the difference among the aerosol mixing state parameters, NF_V and NF_{noBC} agreed with each other with a <0.1 difference ~~smaller than 0.1~~, and both were higher than NF_H by at least 0.1 ~~than~~ NF_H in the moderately polluted period. ~~In detail, compared to~~Compared with NF_{noBC}, NF_V was higher during the heavily polluted period, when the nitrate fraction was the highest ~~and the~~(~30%). The SOA fraction was the lowest (~7%) among all three periods, suggesting that some BC-containing aerosols in this period were also identified as volatile, ~~which is~~ consistent with the fact that the formation of semi-volatile nitrate in ~~the~~ BC-containing particles increases their volatility. However, during the ~~clean~~cleaning period, NF_V was even lower than NF_{noBC}, suggesting that some BC-free aerosols were characterized as low volatile and non-negligible fractions of BC-free aerosols dominated ~~within~~ these less volatile aerosol components, which were likely less volatile organic aerosols~~.~~ (not likely contributed by BC-containing particles with a BC smaller than the SP2 detection limit, because the SF of this type of volatile BC-containing aerosols has an SF lower than 80/200, which is substantially lower than the threshold SF of 0.85 for NF_V calculation). In addition, the MAF values generally agreed with the NF_H during the clean period~~, but~~. However, they were larger than the NF_H during the moderately and heavily polluted periods (by ~0.2) when the POA/SOA fractions were higher~~.~~ (~40% vs. ~35%). POA generally ~~had~~has a lower hygroscopicity than SOA. The critical κ of hydrophilic mode aerosols was 0.07, suggesting that a higher fraction of aerosols had κ below 0.07 (i.e., hydrophobic mode aerosols in this study) during the moderately polluted period. However, under supersaturated conditions, they ~~demonstrated~~demonstrate enhanced hygroscopicity by becoming CCN-active. ~~The~~ NF_H was consistently lower than NF_V and NF_{noBC} (the average difference between NF_H and NF_{noBC} was ~~about~~approximately 0.2~~), especially~~). As mentioned above, NF_H was also lower than MAF during ~~the~~ moderately polluted ~~period, suggesting~~periods, and there may be a significant fraction of volatile BC-free aerosols ~~had~~with hygroscopicity lower than the critical κ value of 0.07 ~~but~~; however, they were still CCN-active and therefore not fully hydrophobic.

The diurnal variations ~~of~~in MAF, NF_H, NF_V, and NF_{noBC}, along with the ~~mass fractions~~MFs of the aerosol chemical ~~compositions~~components during the three periods, are shown in Fig. 4. ~~With the exception of~~ Except for a particle size of 50 nm, the diurnal variations ~~of~~in these four mixing state parameters were generally similar for all measured sizes. The different diurnal variations at a particle size of 50 nm may be due to the different effects of emissions and aging processes on the different aerosol modes, as particles ~~smaller than 100nm were~~<100 nm mainly ~~in a different aerosol mode (~~reside in the Aitken mode~~) to~~ , which is where particles ~~larger than 100nm~~>100 nm mainly reside in the accumulation mode (Wang et al., 2022). For ~~particle sizes larger than~~ particles >100 nm~~,~~ (Fig. 4 and S5), there ~~were peaks~~was a maximum in the afternoon for MAF, NF_H, NF_V, and NF_{noBC}, indicating a peak during this time due to ~~the~~an increase in ~~secondary aerosol~~SA compositions ~~like~~, such as nitrate and SOA, and ~~the~~a decrease ~~of~~in POA and BC. ~~The diurnal~~Diurnal variations ~~of~~in the aerosol mixing state parameters and ~~aerosol~~ chemical compositions were more pronounced ~~in~~during the moderately polluted period. During ~~the~~ heavily polluted ~~period~~periods, the diurnal variation was least pronounced for NF_V and most pronounced for NF_H. In the clean~~-~~air period, there was another ~~peak~~maximum at midnight for MAF and NF_{noBC}, which may be attributed to the diurnal variations ~~of secondary aerosol~~in SA compositions ~~like~~, such as sulfate and SOA, and the decrease ~~of~~in BC and FFOA. The average ~~-~~ size ~~-~~ dependence of the aerosol mixing state parameters ~~in~~over different time ranges during ~~the~~a heavily polluted period is shown in Fig. ~~S3~~S6. It can be seen that the differences among the four parameters were the least from 12:00 to 18:00, with the most SOA and the least POA. This is consistent with the results shown in Fig. 3, where the difference between the MAF and NF_H ~~becomes smaller~~ decreased when the POA fractions ~~are~~were the smallest. R_{exBC} tended to be lower during the daytime, and its diurnal variation was more significant for larger particle sizes. In general, the diurnal variations for R_{exBC} ~~are~~were opposite to those of NF_{noBC} and ~~agree~~agreed better with those of the primary aerosol ~~mass fractions.~~

~~The intercomparisons among MAF, NF_H, NF_V and NF_{noBC} were conducted based on their correlations at different~~MFs. This is because BC particles originate from primary emissions and are mainly mixed externally. After aging in the atmosphere, BC particles can be coated by SAs, resulting in more coated BC particles and fewer externally mixed BC particles. As SAs tend to form on larger particles, the diurnal variations in SA formation may significantly affect the RexBC of larger particle

sizes ~~as~~.

As summarized in Table. S1~~. It's worth noting that~~ , the comparison among MAF, NFH, NFV, and NFnoBC was conducted based on their correlations with different particle sizes. Note that the MAF at SSs of 0.08%, 0.14%%, and 0.22% ~~was~~were used for comparison at ~~particle sizes of~~ 200 ~~nm~~, 150 ~~nm~~, and 100 nm particle sizes. This is because the diameter range of rapid increases in the SPAR curves is determined by aerosol hygroscopicity in this particle size range. The midpoints of the rapidly increasing diameter ranges of the SPAR curves at SSs of 0.08%, 0.14%, and 0.22% were approximately 180 nm, 120 nm, and 90 nm, respectively~~.~~ (as shown in Fig. 2). In general, there were moderate correlations ~~among~~(r=~0.5) between MAF, NF_H, and NF_V, suggesting that a similar particle group contributed to the dominance of CCN-active, hygroscopic, and volatile aerosols ~~are contributed by a similar particle group~~ (Zhang et al., 2016). The ~~consistency of~~agreement between MAF~~-~~ and NF_V was slightly higher than that ~~of~~between MAF~~-~~ and NF_H or between NF_H~~-~~ and NF_V with similar correlation coefficients (~0.65~~) but~~). However, smaller systematic differences (slope and intercept) were much closer to 1 and 0, respectively~~), which~~. This is consistent with the previous finding that a substantial fraction of volatile but less hygroscopic aerosols ~~is~~are CCN-active. ~~At~~For smaller particle ~~size~~sizes, the correlation became weaker~~, while~~ (r=~0.4), whereas the degree of reduction was the ~~least~~lowest for the correlation between MAF and NF_V.

3.3 Impacts of primary aerosol emissions on aerosol mixing states and parameter intercomparisons

~~In~~ Fig. 5~~,~~ presents the correlation between each aerosol mixing state parameter at 200 nm and the ~~mass fraction~~MF of each primary organic aerosol composition during the three periods ~~is presented. In general, these~~. The four mixing state parameters (MAF, NF_H, NF_V, and NF_{noBC}) were negatively correlated with MF_{FFOA} and MF_{BBOA}. However, the ~~correlation~~anticorrelation with MF_{FFOA} (-0.45~-0.74) was much ~~weaker compared to~~stronger than MF_{BBOA}~~.~~ (-0.10~-0.45). Biomass~~-~~burning emissions and fossil fuel emissions are the two major sources of BC in the NCP (Yang et al., 2022), and NF_{noBC} was negatively correlated with MF_{FFOA} (r=-0.49) and weakly correlated (r=-0.18) with MF_{BBOA}, suggesting that fossil fuel ~~emission~~emissions were ~~the more~~ likely the dominant source of BC during

this field campaign. The negative correlation between MAF and MF_{FFOA} was ~~even~~ weaker than that of NF_{noBC} with MF_{FFOA} (-0.62 vs. -0.49). ~~Especially~~In particular, at the same MF_{FFOA}, the MAF was lower than NF_{noBC}, demonstrating that some BC-free particles were CCN-inactive~~,~~ and were likely mainly composed of organic aerosols from fossil fuel combustion ~~emission~~emissions. The negative correlation between NF_V and MF_{FFOA} was slightly weaker than ~~that~~ between NF_{noBC} and MF_{FFOA} (-0.56 vs. -0.49). At the same MF_{FFOA}, NF_{noBC} was close to NF_V, and considering that BC-containing aerosols were dominated by thinly coated BC ~~during~~ most ~~times (as shown in~~ of the time (Fig. 5), this demonstrates that the non-volatile population identified by ~~the~~ V-TDMA was mainly contributed by BC-containing aerosols. NF_H had the lowest negative correlation with MF_{FFOA} (r=-0.74), demonstrating ~~the~~ significant contributions from fossil fuel emissions to nearly hydrophobic aerosol populations. At the same MF_{FFOA}, ~~the~~ NF_H was obviously lower than NF_{noBC} (NF_H and NF_{noBC} were larger and smaller than 0.7 when MF_{FFOA} was larger than 0.1~~, respectively~~), demonstrating that a substantial portion of nearly hydrophobic aerosols was not contributed by BC-containing aerosols~~, but likely by FFOA or BBOA~~ (BC-containing aerosols of 200 nm with BC core smaller than 80 nm which is smaller than the detection limit of SP2 likely to be quite aged in the air, thus not possible to be nearly hydrophobic), but likely by FFOA- or BBOA-dominant aerosols (NF_H also had a negative correlation with MF_{BBOA}). However, the markedly different correlations between MAF ~~with~~and MF_{FFOA} (r=-0.62) and between MAF ~~with~~and MF_{BBOA} (r=-0.2) imply that ~~those~~ nearly hydrophobic but CCN-active aerosols were likely contributed by biomass~~-~~-burning emissions. The correlations between the ratio of thinly coated BC in the total BC-containing particles (R_{exBC}) and the ~~mass fractions~~MFs of BBOA and FFOA are shown in Fig. 6~~, and weak~~. Weak correlations ($r<0.3$) between R_{exBC} ~~with~~and MF_{BBOA} and MF_{FFOA} ~~are~~were observed. However, R_{exBC} tended to increase with MF_{FFOA}, suggesting that BC~~-~~-containing aerosols emitted from fossil fuel combustion tended to be more externally mixed with other aerosol components than those emitted from biomass burning ~~activities~~. These results demonstrate remarkably different mixing states ~~as well as~~and the physical and chemical properties of fossil fuel combustion ~~aerosols~~ and biomass~~-~~-burning aerosols.

The impact of primary emissions on the differences among the four aerosol mixing state parameters ~~is~~ at a particle size of 200 nm was analyzed and is shown in Fig. 7. The difference between NF_{noBC}~~-~~ and NF_H ~~and NF_V~~(NF_{noBC}-NF_H ~~both had strong positive correlations~~) was significantly

positively correlated with MF_{FFOA} and MF_{BBOA} (r>0.5), suggesting that a substantial proportion of POA resided in BC-free aerosols and was volatile, but contributed substantially to nearly hydrophobic aerosols.; as did the differences between NF_V and NF_H (NF_V-NF_H). The mass fractionsMFs of BBOA and FFOA were poorly linkedcorrelated with the differencedifferences between the MAF- and NF_V or (MAF-NF_V), MAF and NF_{noBC} or NF_V(MAF-NF_{noBC}), and NF_V and NF_{noBC} (NF_V-NF_{noBC}) (Fig. S5S7). The difference between MAF-NF_H had a positive correlationwas positively correlated with MF_{BBOA}, further suggesting that BBOA contributed to nearly hydrophobic aerosols under subsaturated conditions;; however, their hygroscopicity was enhanced, and they became CCN-active atunder supersaturated conditions. The correlations between the mixing-state parameters and primary aerosol composition during the campaign and different pollution periods are summarized in Fig. S7.

3.4 Impacts of secondary aerosol formationsSA formation on aerosol mixing states and parameter intercomparisons

The correlations between eachthe aerosol mixing state parameterparameters at 200 nm and the mass fractionMF of each secondary aerosol SA component are presented in Fig. 8 for three periods, and the entire campaign areis presented. The analysis is conducted at only 200 nm, where all four aerosol mixing state parameters were measured to compare the four aerosol mixing state parameters and their relationships with aerosol chemical compositions simultaneously. Generally, MAF, NF_H, NF_V, and NF_{noBC} had aexhibited strong positive correlationcorrelations with ammonium.MF_{NH4} (r>0.5). This is likely due to the fact thatbecause ammonium was mainly formed through the neutralization ofneutralizing sulfuric and nitric acidacids with ammonia, so; therefore, variations in ammonium better represent overall secondary inorganic aerosol formation. As shown in Fig. 3, the secondary inorganic aerosol components dominated over SA (aboutapproximately 50% vs about. approximately 70%), indicating that secondary aerosol formations wereSA formation was primarily composed of secondary inorganic aerosol formation, which explains the weaker correlationscorrelation with SOA seen(r=~0.3), as shown in Fig. 8.

During the clean-air period, when the mass fractionMFs of SOA and sulfate were both above 15%, all four parameters had a strong positive correlation with MF_{SO4} and MF_{SOA} (r>0.5), suggesting that when a clean background airmassair mass with higher fractions of sulfate and SOA prevailed, the

local primary emissions that contributed substantially to BC-containing and less hygroscopic POA aerosols became less significant. The positive correlations between the MAF and ~~secondary aerosol~~SA components have been extensively discussed by Tao et al. (2021), who found that ~~secondary aerosol formations enhance~~SA formation enhances the hygroscopicity of nearly hydrophobic aerosols, thereby increasing CCN activity. This also explains the ~~highest correlations of~~ strong correlation between the NF_H or MAF ~~with~~and ammonium formation. The strong positive correlations between NF_V and ~~secondary aerosol formations~~SA formation (r=~0.6) are consistent with the fact that nitrate dominates ~~secondary aerosol formations~~SA formation during this campaign and ~~nitrate~~ is semi-volatile. For the first time, ~~the~~ strong positive correlations between NF_{noBC} and ~~secondary aerosol formations~~SA formation were ~~revealed. This is because~~observed (r=0.6). NF_{noBC} depends primarily ~~depends~~ on the relative ~~variations of~~variation between BC-containing and BC-free aerosols. The increase in NF_{noBC} at 200 nm as a function of ~~secondary aerosol mass fraction~~the SA MF suggests that ~~secondary aerosol formations~~SAs migrated to a higher fraction of BC-free aerosols smaller than 200 nm to particle size of 200 nm, highlighting that ~~secondary aerosols~~SAs tended to form more quickly on BC-free aerosols than on BC-containing aerosols.

The effects of ~~secondary aerosol~~SA formation on the differences between the four aerosol mixing state parameters were studied and are illustrated in Fig. 9. ~~Differences between~~ The two OOA factors (OOA1 and OOA2) were formed through different chemical pathways. The difference between NF_{noBC}~~-~~ and NF_H ~~and NF_V~~(NF_{noBC}-NF_H ~~both~~) showed a strong negative correlation with MF_{NH4} and MF_{NO3}~~-~~ (mainly -0.6), as did the differences between NF_V and NF_H (NF_V-NF_H). As previously noted~~-~~, NF_H typically ~~had~~has smaller values than NF_V and NF_{noBC}. Thus, a negative correlation ~~with~~between the ~~mass fraction~~MFs of ammonium and nitrate ~~indicates~~indicated that the formation of secondary nitrate ~~results~~resulted in a smaller difference between these mixing state parameters. ~~The~~An increase in the fraction of ammonium nitrate, a pure~~—~~-scattering semi-volatile compound with strong hygroscopicity, can render the aerosol population more dominated by particles with strong volatility and hygroscopicity. ~~This~~As the secondary inorganic aerosol components increase, this can result in a smaller difference between NFnoBC, NFH, and NFV ~~as the secondary inorganic aerosol components increases.~~ .

Furthermore, the difference between NF_V~~-~~ and NF_H showed a positive correlation with MF_{OOA2} and a negative correlation with MF_{OOA1}, indicating different volatility and hygroscopicity of the two SOA factors. The ~~variations in the difference~~differences between NF_V and NF_H ~~with~~concerning the ~~mass fraction~~MF of OOA1 and OOA2 are shown in Fig. 9(e) and (f~~).~~), respectively. As previously noted, NF_V was generally higher than NF_H, and the difference between the two ~~decreases~~decreased with ~~an increase in~~increasing MF_{OOA1}, which ~~were~~was generally smaller than 0.3. This suggests that the formation of OOA1 enhances the hygroscopicity of volatile particles, which aligns with the highest oxidation state of OOA1 (higher O/C but lower H/C compared to OOA2~~), which had~~) and has a significant and overall positive impact on aerosol hygroscopicity (Cerully et al., 2015; Thalman et al., 2017; Zhang et al., 2023). A positive correlation ~~is seen~~was observed between NF_V and MF_{OOA2} (r=~0.25~~), whereas~~).

In contrast, the correlation between NF_H and MF_{OOA2} ~~is~~was weak (R ~~is~~was close to 0), implying that OOA2 might be semi-volatile but only weakly hygroscopic, which could contribute to NF_V being higher than NF_H as OOA1 increases. The difference between NF_{noBC}~~-~~ and NF_V ~~is~~(NF_{noBC}-NF_V) was negatively correlated with MF_{NO3}, which is consistent with the semi-volatile nature of nitrate. The negative correlation between NF_{noBC}-NF_V and MF_{OOA2} indicates that the difference is smaller when there is more OOA2, implying that OOA2 ~~are~~is also a semi-volatile ~~compounds~~compound and ~~were~~is likely formed mainly on BC-free particles. The correlations between the ~~difference~~differences between NF_V-MAF and NF_{noBC}-MAF and the ~~mass fraction~~MF of each ~~secondary aerosol~~SA composition ~~are much~~were very weak. The impacts of ~~secondary aerosol~~SA formation on BC mixing states are ~~depicted~~shown in Fig. ~~S4~~S8. In general, the ~~number fraction~~NF of thinly coated BC has a negative correlation with SIA and a weak association with SOA, suggesting that SIA formation mainly enhances the thickness of ~~BC coating~~the BC coating. The correlations between the mixing state parameters and SA composition during the campaign and different pollution periods are summarized in Fig. S9.

In addition to ~~the~~ changes in the ~~mass fractions~~MFs of ~~secondary aerosol~~SA compositions, the accumulation of SA pollution ~~due to secondary aerosols~~ may ~~also~~ provide ~~insight~~insights into the impact of ~~secondary aerosol formations~~SA formation on aerosol mixing states. As shown in Fig. 10 (a), during the heavily polluted periods, there were two distinct pollution accumulation processes from ~~Oct~~the 23rd~~-~~ to ~~Oct~~the 27th of October and from ~~Oct 28~~rd the 28th to ~~Oct~~the 31st of October,

respectively. During the pollution accumulation process, the mass concentration of ~~secondary aerosols~~SAs increased by approximately three ~~times~~-fold, indicating the rapid formation of secondary compositions and ~~causing~~ a significant ~~rise in PM~~increase in non-refractory PM_1 (NR-PM_1) mass concentration. Fig. 10 (b) and (c) ~~illustrates~~illustrate that this increase in ~~secondary aerosols led to a significant enhancement of~~SAs significantly enhanced aerosol mixing state parameters, including MAF, NF_V, NF_H, and NF_{noBC}, which ~~rose~~increased from ~~about~~approximately 0.5 to ~~about~~ 0.8 with evident diurnal variations. This highlights the impact of ~~secondary aerosol formations on~~SA formation on the aerosol mixing states and the importance of studying the pollution accumulation processes of ~~secondary aerosols.~~SAs. The enhancements ~~of~~in the different aerosol mixing state parameters during the pollution accumulation process were not uniform. MAF and NF_H initially ~~showed~~exhibited lower values ~~compared to~~than NF_V and NF_{noBC}~~, but~~; however, their later enhancement was stronger than that of NF_{noBC}. Fig. 10 (d) and (e) show the difference between NF_{noBC} and NF_V at 200 ~~nm~~ and 300 nm as a function of ~~secondary aerosol~~SA mass concentrations during these two pollution periods, which clearly ~~displays~~shows how, during ~~secondary aerosol formations~~SA formation, NF_V became higher than NF_{noBC} while NF_V ~~kept~~remained close to ~~NF_{noBC} plus~~ the ~~number fraction~~NF of thickly coated BC-containing aerosols~~. The~~ (NF_{CBC}) plus NF_{noBC} (NF_{CBC}+NF_{CBC}). These results suggest that ~~secondary aerosol~~SA formation increases the volatility of BC-free and BC-containing aerosols, leading to an increased NF_V compared ~~to~~with NF_{noBC}. ~~And almost~~Almost all BC-free particles and some BC-containing aerosols ~~became~~become volatile during the ~~pollution~~ accumulation ~~process~~of pollution.

4. Conclusions

The aerosol mixing state is one of the most important physicochemical properties of aerosol particles~~, which has significant impacts on the~~ and significantly affects their optical properties and the CCN activity of aerosol particles. ~~Aerosol~~The aerosol mixing ~~state varies largely under~~states vary significantly with complex aerosol emissions and atmospheric transformations. In this study, aerosol mixing states derived from CCN activity, hygroscopicity, volatility, and BC ~~particles~~particle observations, along with their relationship to primary ~~aerosols~~aerosol emissions and ~~secondary aerosol formations~~SA formation, were systematically analyzed based on simultaneous measurements of ~~a~~ CCNC, ~~a~~ H/VTDMA, and ~~a~~ SP2. Statistical analysis demonstrated that the ~~number fraction~~NFs of

CCN-active, hygroscopic, and volatile particles were generally positively correlated ~~to one another~~ and ~~were~~mainly contributed ~~mainly~~ by BC-free aerosols. Therefore, ~~NF_{noBC}, MAF, NF_H, and NF_V~~four mixing state parameters were all negatively correlated to either ~~MF_{FFOA}~~the MFs of BBOA or ~~MF_{BBOA},~~FFOA because fossil fuel combustion and biomass burning were the two major sources of BC-containing aerosols during this field campaign. However, the differences ~~among~~between these mixing state parameters ~~varied much~~vary significantly under different conditions.

The intercomparison results highlight the differences in the aerosol mixing states and ~~physiochemical~~physicochemical properties caused by fossil fuel combustion and biomass~~-~~-burning emissions. The CCN and SP2 measurements showed that CCN-inactive~~,~~ BC-free particles were mainly produced by fossil fuel combustion. ~~On the other hand, the~~In contrast, a comparison between the VTDMA and SP2 measurements indicated that the non-volatile aerosols ~~were~~ mostly ~~composed of~~comprised BC-containing particles. The comparison between HTDMA and SP2 measurements revealed that a significant proportion of nearly hydrophobic aerosols was not from BC-containing particles~~,~~ but from fossil fuel combustion or biomass~~-~~-burning~~-~~-dominated organic aerosols. The correlation between the CCNC and HTDMA measurements also showed that nearly hydrophobic, BC-free aerosols ~~can~~could become CCN-active under supersaturated conditions and ~~were~~are tightly linked to biomass~~-~~-burning emissions. This suggests that biomass~~-~~-burning aerosols ~~might~~may exhibit different ~~hygroscopicity~~hygroscopicities under sub- and ~~super- saturated~~supersaturated conditions (Bougiatioti et al., 2016). Furthermore, the correlation analysis between SP2 measurements and ~~mass fractions~~the MFs of BBOA and FFOA indicated that BC-containing aerosols from fossil fuel combustion ~~tend~~tended to be more externally mixed with other aerosol compositions ~~compared to~~than those from biomass burning activities.

~~Other than~~In addition to primary aerosol emissions, ~~secondary aerosol formations~~ SA formation also ~~exerted significant~~significantly impacts ~~on~~ variations ~~of~~in aerosol mixing states. During this campaign, ~~the secondary aerosol~~SA formation was dominated by nitrate and SOA production, which ~~have~~had markedly different impacts on the aerosol mixing states ~~due~~owing to their different physical properties and formation pathways. NF_{noBC}, MAF, NF_H, and NF_V were all positively correlated with the nitrate and SOA ~~mass fractions~~MFs, revealing much stronger correlations ~~to~~with SOA than ~~with~~ nitrate. This is consistent with the semi-volatile but highly hygroscopic properties of ~~nitrate~~nitrates.

The high correlation coefficient between NF_{noBC} and the ~~mass fractions~~MFs of ~~secondary aerosols~~SAs at 200 ~~nm~~ and 300 nm suggests that ~~secondary aerosol~~SA formation led to the migration of BC-free aerosols towards larger diameters more quickly than that of BC-containing aerosols. This ~~outcome~~result reveals that ~~secondary aerosols~~ SAs formed more rapidly on BC-free ~~aerosols~~ than on BC-containing aerosols, which ~~is in line~~aligns with the ~~BC-containing aerosols'~~ hydrophobic nature of BC-containing aerosols that ~~does~~do not favor aqueous ~~secondary aerosol~~SA formation. Moreover, as the ~~mass fractions~~MFs of nitrate or ammonium increased, the differences ~~among~~between the mixing -state parameters (NF_{noBC}, MAF, NF_H, and NF_V) ~~mostly~~ decreased ~~due to~~because of the hygroscopic and semi-volatile nature of ammonium nitrate. However, the two resolved SOA factors exhibited different impacts on ~~NF_V~~ the differences between NF_V and NF_H; (NF_V-NF_H), and their correlations with NF_V and NF_H revealed that OOA1 was more hygroscopic but less volatile, suggesting distinct formation mechanisms for ~~the~~these two OOA factors during the field campaign.

The findings of this study highlight the markedly different effects of primary emissions and ~~secondary aerosol formations~~SA formation on aerosol mixing states and suggest that comparisons of aerosol mixing states obtained using various techniques are useful for gaining insights into the hygroscopicity, volatility, and CCN activity of different aerosols. These comparisons ~~can~~ also indicate the ~~impacts~~impact of ~~secondary aerosol formations~~SA formation on aerosol physical properties, which can help ~~to~~ understand the pathways of ~~secondary aerosol~~SA formation. However, it is important to be cautious in the application of aerosol mixing state parameters~~, as~~ because the suitability of VTDMA-derived mixing state parameters ~~in~~for representing BC mixing states is largely dependent on the composition and mass of ~~secondary aerosols~~the SAs.

Data availability. The data used in this study are available from the corresponding author upon request Ye Kuang (kuangye@jnu.edu.cn) and Li Liu (liul@gd121.cn)

Competing interests. The authors declare that they have no conflict of interest.

Author Contributions.

YK and WY planned this campaign and YK designed the aerosol experiments and conceived this research together with JC, and JC wrote the manuscript. JC performed measurements of CCNC, BL performed measurements of SP2 and analyzed SP2 datasets with the help of GZ, WQ and YL performed AMS measurements, LL performed HV-TDMA measurements and conducted post-data processing as well as some of data analysis. BX, HX, MMZ, HZ and SR participated this campaign and helped instruments maintenance. GZ provided full support for the campaign. All authors contributed to discussions and revisions of this paper.

Financial supports. This work is supported by National Natural Science Foundation of China (42175083, 42175127, 42275066~~). The~~), the Guangzhou Science and Information Technology Bureau Project (2023A04J0941), the Guangdong Provincial Key Research and Development Program (grant no. 2020B1111360003), the Science and Technology Innovation Team Plan of Guangdong Meteorological Bureau (grant no. GRMCTD202003).

References

Adachi, K., Sedlacek, A. J., Kleinman, L., Chand, D., Hubbe, J. M., and Buseck, P. R.: Volume changes upon heating of aerosol particles from biomass burning using transmission electron microscopy, Aerosol Science and Technology, 52, 46–56, https://doi.org/10.1080/02786826.2017.1373181, 2018.

Adachi, K., Sedlacek, A. J., Kleinman, L., Springston, S. R., Wang, J., Chand, D., Hubbe, J. M., Shilling, J. E., Onasch, T. B., Kinase, T., Sakata, K., Takahashi, Y., and Buseck, P. R.: Spherical tarball particles form through rapid chemical and physical changes of organic matter in biomass-burning smoke, Proceedings of the National Academy of Sciences, 116, 19336–19341, https://doi.org/10.1073/pnas.1900129116, 2019.

Bond, T. C., Doherty, S. J., Fahey, D. W., Forster, P. M., Berntsen, T., DeAngelo, B. J., Flanner, M. G., Ghan, S., Kaercher, B., Koch, D., Kinne, S., Kondo, Y., Quinn, P. K., Sarofim, M. C., Schultz, M. G., Schulz, M., Venkataraman, C., Zhang, H., Zhang, S., Bellouin, N., Guttikunda, S. K., Hopke, P. K., Jacobson, M. Z., Kaiser, J. W., Klimont, Z., Lohmann, U., Schwarz, J. P., Shindell, D., Storelvmo, T., Warren, S. G., and Zender, C. S.: Bounding the role of black carbon in the climate system: A scientific assessment, Journal of Geophysical Research-Atmospheres, 118, 5380–5552, https://doi.org/10.1002/jgrd.50171, 2013.

Bougiatioti, A., Bezantakos, S., Stavroulas, I., Kalivitis, N., Kokkalis, P., Biskos, G., Mihalopoulos, N., Papayannis, A., and Nenes, A.: Biomass-burning impact on CCN number, hygroscopicity and cloud formation during summertime in the eastern Mediterranean, Atmos. Chem. Phys., 16, 7389–7409, https://doi.org/10.5194/acp-16-7389-2016, 2016.

Cai, M., Tan, H., Chan, C. K., Mochida, M., Hatakeyama, S., Kondo, Y., Schurman, M. I., Xu, H., Li, F., Shimada, K., Li, L., Deng, Y., Yai, H., Matsuki, A., Qin, Y., and Zhao, J.: Comparison of Aerosol Hygroscopcity, Volatility, and Chemical Composition between a Suburban Site in the Pearl River Delta Region and a Marine Site in Okinawa, Aerosol and Air Quality Research, 17, 3194–3208, https://doi.org/10.4209/aaqr.2017.01.0020, 2017.

Canagaratna, M. R., Jimenez, J. L., Kroll, J. H., Chen, Q., Kessler, S. H., Massoli, P., Hildebrandt Ruiz, L., Fortner, E., Williams, L. R., Wilson, K. R., Surratt, J. D., Donahue, N. M., Jayne, J. T., and Worsnop, D. R.: Elemental ratio measurements of organic compounds using aerosol mass spectrometry: characterization, improved calibration, and implications, Atmos. Chem. Phys., 15, 253–272, https://doi.org/10.5194/acp-15-253-2015, 2015.

Cerully, K. M., Bougiatioti, A., Hite Jr., J. R., Guo, H., Xu, L., Ng, N. L., Weber, R., and Nenes, A.: On the link between hygroscopicity, volatility, and oxidation state of ambient and water-soluble aerosols in the southeastern United States, Atmos. Chem. Phys., 15, 8679–8694, https://doi.org/10.5194/acp-15-8679-2015, 2015.

Chen, C., Qiu, Y., Xu, W., He, Y., Li, Z., Sun, J., Ma, N., Xu, W., Pan, X., Fu, P., Wang, Z., and Sun, Y.: Primary Emissions and Secondary Aerosol Processing During Wintertime in Rural Area of North China Plain, Journal of Geophysical Research: Atmospheres, 127, e2021JD035430, https://doi.org/10.1029/2021JD035430, 2022.

Chen, J., Budisulistiorini, S. H., Miyakawa, T., Komazaki, Y., and Kuwata, M.: Secondary aerosol formation promotes water uptake by organic-rich wildfire haze particles in equatorial Asia, Atmos. Chem. Phys., 18, 7781–7798, https://doi.org/10.5194/acp-18-7781-2018, 2018.

Cheng, Y. F., Su, H., Rose, D., Gunthe, S. S., Berghof, M., Wehner, B., Achtert, P., Nowak, A., Takegawa, N., Kondo, Y., Shiraiwa, M., Gong, Y. G., Shao, M., Hu, M., Zhu, T., Zhang, Y. H., Carmichael, G. R., Wiedensohler, A., Andreae, M. O., and Pöschl, U.: Size-resolved measurement of the mixing state of soot in the megacity Beijing, China: diurnal cycle, aging and parameterization, Atmos. Chem. Phys., 12, 4477–4491, https://doi.org/10.5194/acp-12-4477-2012, 2012.

Ching, J., Fast, J., West, M., and Riemer, N.: Metrics to quantify the importance of mixing state for CCN activity, Atmos. Chem. Phys., 17, 7445–7458, https://doi.org/10.5194/acp-17-7445-2017, 2017.

Ching, J., Adachi, K., Zaizen, Y., Igarashi, Y., and Kajino, M.: Aerosol mixing state revealed by transmission electron microscopy pertaining to cloud formation and human airway deposition, npj Climate and Atmospheric Science, 2, 22, https://doi.org/10.1038/s41612-019-0081-9, 2019.

Deng, Z. Z., Zhao, C. S., Ma, N., Liu, P. F., Ran, L., Xu, W. Y., Chen, J., Liang, Z., Liang, S., Huang, M. Y., Ma, X. C., Zhang, Q., Quan, J. N., Yan, P., Henning, S., Mildenberger, K., Sommerhage, E., Schäfer, M., Stratmann, F., and Wiedensohler, A.: Size-resolved and bulk activation properties of aerosols in the North China Plain, Atmos. Chem. Phys., 11, 3835–3846, https://doi.org/10.5194/acp-11-3835-2011, 2011.

Deng, Z. Z., Zhao, C. S., Ma, N., Ran, L., Zhou, G. Q., Lu, D. R., and Zhou, X. J.: An examination of parameterizations for the CCN number concentration based on in situ measurements of aerosol activation properties in the North China Plain, Atmos. Chem. Phys., 13, 6227–6237, https://doi.org/10.5194/acp-13-6227-2013, 2013.

Drinovec, L., Močnik, G., Zotter, P., Prévôt, A. S. H., Ruckstuhl, C., Coz, E., Rupakheti, M., Sciare, J., Müller, T., Wiedensohler, A., and Hansen, A. D. A.: The "dual-spot" Aethalometer: an improved measurement of aerosol black carbon with real-time loading compensation, Atmos. Meas. Tech., 8, 1965–1979, https://doi.org/10.5194/amt-8-1965-2015, 2015.

Ervens, B.: Modeling the Processing of Aerosol and Trace Gases in Clouds and Fogs, Chemical Reviews, 115, 4157–4198, https://doi.org/10.1021/cr5005887, 2015.

Farmer, D. K., Cappa, C. D., and Kreidenweis, S. M.: Atmospheric Processes and Their Controlling Influence on Cloud Condensation Nuclei Activity, Chemical Reviews, 115, 4199–4217, https://doi.org/10.1021/cr5006292, 2015.

Fierce, L., Riemer, N., and Bond, T. C.: Toward Reduced Representation of Mixing State for Simulating Aerosol Effects on Climate, Bulletin of the American Meteorological Society, 98, 971–980, https://doi.org/10.1175/BAMS-D-16-0028.1, 2017.

Fu, Y., Peng, X., Sun, W., Hu, X., Wang, D., Yang, Y., Guo, Z., Wang, Y., Zhang, G., Zhu, J., Ou, J., Shi, Z., Wang, X., and Bi, X.: Impact of Cloud Process in the Mixing State and Microphysical Properties of Soot Particles: Implications in Light Absorption Enhancement, Journal of Geophysical Research: Atmospheres, n/a, e2022JD037169, https://doi.org/10.1029/2022JD037169, 2022.

Gysel, M., Laborde, M., Olfert, J. S., Subramanian, R., and Gröhn, A. J.: Effective density of Aquadag and fullerene soot black carbon reference materials used for SP2 calibration, Atmos. Meas. Tech., 4, 2851–2858, https://doi.org/10.5194/amt-4-2851-2011, 2011.

Herich, H., Kammermann, L., Gysel, M., Weingartner, E., Baltensperger, U., Lohmann, U., and Cziczo, D. J.: In situ determination of atmospheric aerosol composition as a function of hygroscopic growth, Journal of Geophysical Research: Atmospheres, 113, https://doi.org/10.1029/2008JD009954, 2008.

Herich, H., Kammermann, L., Friedman, B., Gross, D. S., Weingartner, E., Lohmann, U., Spichtinger, P., Gysel, M., Baltensperger, U., and Cziczo, D. J.: Subarctic atmospheric aerosol composition: 2. Hygroscopic growth properties, Journal of Geophysical Research: Atmospheres, 114, https://doi.org/10.1029/2008JD011574, 2009.

Hong, J., Äijälä, M., Häme, S. A. K., Hao, L., Duplissy, J., Heikkinen, L. M., Nie, W., Mikkilä, J., Kulmala, M., Prisle, N. L., Virtanen, A., Ehn, M., Paasonen, P., Worsnop, D. R., Riipinen, I., Petäjä, T., and Kerminen, V.-M.: Estimates of the organic aerosol volatility in a boreal forest using two independent methods, Atmos. Chem. Phys., 17, 4387–4399, https://doi.org/10.5194/acp-17-4387-2017, 2017.

Jayne, J. T., Leard, D. C., Zhang, X., Davidovits, P., Smith, K. A., Kolb, C. E., and Worsnop, D. R.: Development of an Aerosol Mass Spectrometer for Size and Composition Analysis of Submicron Particles, Aerosol Science and Technology, 33, 49–70, https://doi.org/10.1080/027868200410840, 2000.

Jiang, X., Tao, J., Kuang, Y., Hong, J., and Ma, N.: Mathematical derivation and physical interpretation of particle size-resolved activation ratio based on particle hygroscopicity distribution: Application on global characterization of CCN activity, Atmospheric Environment, 246, 118137, https://doi.org/10.1016/j.atmosenv.2020.118137, 2021.

Jurányi, Z., Tritscher, T., Gysel, M., Laborde, M., Gomes, L., Roberts, G., Baltensperger, U., and Weingartner, E.: Hygroscopic mixing state of urban aerosol derived from size-resolved cloud condensation nuclei measurements during the MEGAPOLI campaign in Paris, Atmos. Chem. Phys., 13, 6431–6446, https://doi.org/10.5194/acp-13-6431-2013, 2013.

Kawana, K., Nakayama, T., and Mochida, M.: Hygroscopicity and CCN activity of atmospheric aerosol particles and their relation to organics: Characteristics of urban aerosols in Nagoya, Japan, Journal of Geophysical Research: Atmospheres, 121, 4100–4121, https://doi.org/10.1002/2015jd023213, 2016.

Kim, N., Yum, S. S., Park, M., Park, J. S., Shin, H. J., and Ahn, J. Y.: Hygroscopicity of urban aerosols and its link to size-resolved chemical composition during spring and summer in Seoul, Korea, Atmos. Chem. Phys., 20, 11245–11262, https://doi.org/10.5194/acp-20-11245-2020, 2020.

Kuang, Y., Zhao, C. S., Tao, J. C., and Ma, N.: Diurnal variations of aerosol optical properties in the North China Plain and their influences on the estimates of direct aerosol radiative effect, Atmos. Chem. Phys., 15, 5761–5772, https://doi.org/10.5194/acp-15-5761-2015, 2015.

Kuang, Y., He, Y., Xu, W., Yuan, B., Zhang, G., Ma, Z., Wu, C., Wang, C., Wang, S., Zhang, S., Tao, J., Ma, N., Su, H., Cheng, Y., Shao, M., and Sun, Y.: Photochemical Aqueous-Phase Reactions

Induce Rapid Daytime Formation of Oxygenated Organic Aerosol on the North China Plain, Environmental Science & Technology, 54, 3849–3860, https://doi.org/10.1021/acs.est.9b06836, 2020.

Kuang, Y., Huang, S., Xue, B., Luo, B., Song, Q., Chen, W., Hu, W., Li, W., Zhao, P., Cai, M., Peng, Y., Qi, J., Li, T., Wang, S., Chen, D., Yue, D., Yuan, B., and Shao, M.: Contrasting effects of secondary organic aerosol formations on organic aerosol hygroscopicity, Atmos. Chem. Phys., 21, 10375–10391, https://doi.org/10.5194/acp-21-10375-2021, 2021.

Kuwata, M. and Kondo, Y.: Dependence of size-resolved CCN spectra on the mixing state of nonvolatile cores observed in Tokyo, Journal of Geophysical Research: Atmospheres, 113, https://doi.org/10.1029/2007JD009761, 2008.

Kuwata, M., Kondo, Y., Mochida, M., Takegawa, N., and Kawamura, K.: Dependence of CCN activity of less volatile particles on the amount of coating observed in Tokyo, Journal of Geophysical Research: Atmospheres, 112, https://doi.org/10.1029/2006JD007758, 2007.

Lack, D. A., Langridge, J. M., Bahreini, R., Cappa, C. D., Middlebrook, A. M., and Schwarz, J. P.: Brown carbon and internal mixing in biomass burning particles, Proceedings of the National Academy of Sciences, 109, 14802–14807, https://doi.org/10.1073/pnas.1206575109, 2012.

Lance, S., Nenes, A., Medina, J., and Smith, J. N.: Mapping the operation of the DMT continuous flow CCN counter, Aerosol science and technology, 40, 242–254, 2006.

Lance, S., Raatikainen, T., Onasch, T. B., Worsnop, D. R., Yu, X. Y., Alexander, M. L., Stolzenburg, M. R., McMurry, P. H., Smith, J. N., and Nenes, A.: Aerosol mixing state, hygroscopic growth and cloud activation efficiency during MIRAGE 2006, Atmos. Chem. Phys., 13, 5049–5062, https://doi.org/10.5194/acp-13-5049-2013, 2013.

Lata, N. N., Zhang, B., Schum, S., Mazzoleni, L., Brimberry, R., Marcus, M. A., Cantrell, W. H., Fialho, P., Mazzoleni, C., and China, S.: Aerosol Composition, Mixing State, and Phase State of Free Tropospheric Particles and Their Role in Ice Cloud Formation, ACS Earth Space Chem., 5, 3499–3510, https://doi.org/10.1021/acsearthspacechem.1c00315, 2021.

Lee, A. K. Y., Rivellini, L.-H., Chen, C.-L., Liu, J., Price, D. J., Betha, R., Russell, L. M., Zhang, X., and Cappa, C. D.: Influences of Primary Emission and Secondary Coating Formation on the Particle Diversity and Mixing State of Black Carbon Particles, Environ. Sci. Technol., 53, 9429–9438, https://doi.org/10.1021/acs.est.9b03064, 2019.

Li, G., Su, H., Ma, N., Tao, J., Kuang, Y., Wang, Q., Hong, J., Zhang, Y., Kuhn, U., and Zhang, S.: Multiphase chemistry experiment in Fogs and Aerosols in the North China Plain (McFAN): integrated analysis and intensive winter campaign 2018, Faraday Discussions, 2021.

Liu, D., Joshi, R., Wang, J., Yu, C., Allan, J. D., Coe, H., Flynn, M. J., Xie, C., Lee, J., Squires, F., Kotthaus, S., Grimmond, S., Ge, X., Sun, Y., and Fu, P.: Contrasting physical properties of black carbon in urban Beijing between winter and summer, Atmos. Chem. Phys., 19, 6749–6769, https://doi.org/10.5194/acp-19-6749-2019, 2019.

Liu, D., Li, S., Hu, D., Kong, S., Cheng, Y., Wu, Y., Ding, S., Hu, K., Zheng, S., Yan, Q., Zheng, H., Zhao, D., Tian, P., Ye, J., Huang, M., and Ding, D.: Evolution of Aerosol Optical Properties from Wood Smoke in Real Atmosphere Influenced by Burning Phase and Solar Radiation, Environ. Sci. Technol., 55, 5677–5688, https://doi.org/10.1021/acs.est.0c07569, 2021.

Liu, K., Zhang, C., Cheng, Y., Liu, C., Zhang, H., Zhang, G., Sun, X., and Mu, Y.: Serious BTEX pollution in rural area of the North China Plain during winter season, Journal of Environmental Sciences, 30, 186–190, https://doi.org/10.1016/j.jes.2014.05.056, 2015.

Liu, P. F., Zhao, C. S., Göbel, T., Hallbauer, E., Nowak, A., Ran, L., Xu, W. Y., Deng, Z. Z., Ma, N., and Mildenberger, K.: Hygroscopic properties of aerosol particles at high relative humidity and their diurnal variations in the North China Plain, Atmos. Chem. Phys, 11, 3479–3494, 2011.

Luo, B., Kuang, Y., Huang, S., Song, Q., Hu, W., Li, W., Peng, Y., Chen, D., Yue, D., Yuan, B., and Shao, M.: Parameterizations of size distribution and refractive index of biomass burning organic aerosol with black carbon content, Atmos. Chem. Phys., 22, 12401–12415, https://doi.org/10.5194/acp-22-12401-2022, 2022.

Ma, N., Zhao, C. S., Müller, T., Cheng, Y. F., Liu, P. F., Deng, Z. Z., Xu, W. Y., Ran, L., Nekat, B., van Pinxteren, D., Gnauk, T., Müller, K., Herrmann, H., Yan, P., Zhou, X. J., and Wiedensohler, A.: A new method to determine the mixing state of light absorbing carbonaceous using the measured aerosol optical properties and number size distributions, Atmos. Chem. Phys., 12, 2381–2397, https://doi.org/10.5194/acp-12-2381-2012, 2012.

Ma, N., Zhao, C., Tao, J., Wu, Z., Kecorius, S., Wang, Z., Größ, J., Liu, H., Bian, Y., Kuang, Y., Teich, M., Spindler, G., Müller, K., van Pinxteren, D., Herrmann, H., Hu, M., and Wiedensohler, A.: Variation of CCN activity during new particle formation events in the North China Plain, Atmos. Chem. Phys., 16, 8593–8607, https://doi.org/10.5194/acp-16-8593-2016, 2016.

Matsui, H., Hamilton, D. S., and Mahowald, N. M.: Black carbon radiative effects highly sensitive to emitted particle size when resolving mixing-state diversity, Nature Communications, 9, 3446, https://doi.org/10.1038/s41467-018-05635-1, 2018.

Mei, F., Hayes, P. L., Ortega, A., Taylor, J. W., Allan, J. D., Gilman, J., Kuster, W., de Gouw, J., Jimenez, J. L., and Wang, J.: Droplet activation properties of organic aerosols observed at an urban site during CalNex-LA, Journal of Geophysical Research-Atmospheres, 118, 2903–2917, https://doi.org/10.1002/jgrd.50285, 2013.

Metcalf, A. R., Craven, J. S., Ensberg, J. J., Brioude, J., Angevine, W., Sorooshian, A., Duong, H. T., Jonsson, H. H., Flagan, R. C., and Seinfeld, J. H.: Black carbon aerosol over the Los Angeles Basin during CalNex, Journal of Geophysical Research: Atmospheres, 117, https://doi.org/10.1029/2011JD017255, 2012.

Middlebrook, A. M., Bahreini, R., Jimenez, J. L., and Canagaratna, M. R.: Evaluation of Composition-Dependent Collection Efficiencies for the Aerodyne Aerosol Mass Spectrometer using Field Data, Aerosol Science and Technology, 46, 258–271, https://doi.org/10.1080/02786826.2011.620041, 2012.

Moffet, R. C., O'Brien, R. E., Alpert, P. A., Kelly, S. T., Pham, D. Q., Gilles, M. K., Knopf, D. A., and Laskin, A.: Morphology and mixing of black carbon particles collected in central California during the CARES field study, Atmos. Chem. Phys., 16, 14515–14525, https://doi.org/10.5194/acp-16-14515-2016, 2016.

Mohr, C., Huffman, J. A., Cubison, M. J., Aiken, A. C., Docherty, K. S., Kimmel, J. R., Ulbrich, I. M., Hannigan, M., and Jimenez, J. L.: Characterization of Primary Organic Aerosol Emissions from

Meat Cooking, Trash Burning, and Motor Vehicles with High-Resolution Aerosol Mass Spectrometry and Comparison with Ambient and Chamber Observations, Environ. Sci. Technol., 43, 2443–2449, https://doi.org/10.1021/es8011518, 2009.

Moteki, N. and Kondo, Y.: Effects of Mixing State on Black Carbon Measurements by Laser-Induced Incandescence, Aerosol Science and Technology, 41, 398–417, https://doi.org/10.1080/02786820701199728, 2007.

Nordmann, S., Cheng, Y. F., Carmichael, G. R., Yu, M., Denier van der Gon, H. A. C., Zhang, Q., Saide, P. E., Pöschl, U., Su, H., Birmili, W., and Wiedensohler, A.: Atmospheric black carbon and warming effects influenced by the source and absorption enhancement in central Europe, Atmos. Chem. Phys., 14, 12683–12699, https://doi.org/10.5194/acp-14-12683-2014, 2014.

Paatero, P. and Tapper, U.: Positive matrix factorization: A non-negative factor model with optimal utilization of error estimates of data values, Environmetrics, 5, 111–126, https://doi.org/10.1002/env.3170050203, 1994.

Peng, J., Hu, M., Guo, S., Du, Z., Zheng, J., Shang, D., Levy Zamora, M., Zeng, L., Shao, M., Wu, Y.-S., Zheng, J., Wang, Y., Glen, C. R., Collins, D. R., Molina, M. J., and Zhang, R.: Markedly enhanced absorption and direct radiative forcing of black carbon under polluted urban environments, Proceedings of the National Academy of Sciences, 113, 4266–4271, https://doi.org/10.1073/pnas.1602310113, 2016.

Philippin, S., Wiedensohler, A., and Stratmann, F.: Measurements of non-volatile fractions of pollution aerosols with an eight-tube volatility tandem differential mobility analyzer (VTDMA-8), Journal of Aerosol Science, 35, 185–203, https://doi.org/10.1016/j.jaerosci.2003.07.004, 2004.

Ren, J., Zhang, F., Wang, Y., Collins, D., Fan, X., Jin, X., Xu, W., Sun, Y., Cribb, M., and Li, Z.: Using different assumptions of aerosol mixing state and chemical composition to predict CCN concentrations based on field measurements in urban Beijing, Atmospheric Chemistry and Physics, 18, 6907–6921, https://doi.org/10.5194/acp-18-6907-2018, 2018.

Riemer, N., Ault, A. P., West, M., Craig, R. L., and Curtis, J. H.: Aerosol Mixing State: Measurements, Modeling, and Impacts, Reviews of Geophysics, 57, 187–249, https://doi.org/10.1029/2018RG000615, 2019.

Roberts, G. C. and Nenes, A.: A continuous-flow streamwise thermal-gradient CCN chamber for atmospheric measurements, Aerosol science and technology, 39, 206–221, 2005.

Rose, D., Gunthe, S. S., Mikhailov, E., Frank, G. P., Dusek, U., Andreae, M. O., and Pöschl, U.: Calibration and measurement uncertainties of a continuous-flow cloud condensation nuclei counter (DMT-CCNC): CCN activation of ammonium sulfate and sodium chloride aerosol particles in theory and experiment, Atmos. Chem. Phys., 8, 1153–1179, 2008.

Rose, D., Nowak, A., Achtert, P., Wiedensohler, A., Hu, M., Shao, M., Zhang, Y., Andreae, M. O., and Poschl, U.: Cloud condensation nuclei in polluted air and biomass burning smoke near the mega-city Guangzhou, China - Part 1: Size-resolved measurements and implications for the modeling of aerosol particle hygroscopicity and CCN activity, Atmos. Chem. Phys., 10, 3365–3383, 2010.

Rose, D., Gunthe, S. S., Su, H., Garland, R. M., Yang, H., Berghof, M., Cheng, Y. F., Wehner, B., Achtert, P., Nowak, A., Wiedensohler, A., Takegawa, N., Kondo, Y., Hu, M., Zhang, Y., Andreae,

M. O., and Poschl, U.: Cloud condensation nuclei in polluted air and biomass burning smoke near the mega-city Guangzhou, China -Part 2: Size-resolved aerosol chemical composition, diurnal cycles, and externally mixed weakly CCN-active soot particles, Atmos. Chem. Phys., 11, 2817–2836, https://doi.org/10.5194/acp-11-2817-2011, 2011.

Saha, P. K., Khlystov, A., and Grieshop, A. P.: Downwind evolution of the volatility and mixing state of near-road aerosols near a US interstate highway, Atmos. Chem. Phys., 18, 2139–2154, https://doi.org/10.5194/acp-18-2139-2018, 2018.

Sedlacek, A. J., Lewis, E. R., Kleinman, L., Xu, J., and Zhang, Q.: Determination of and evidence for non-core-shell structure of particles containing black carbon using the Single-Particle Soot Photometer (SP2), Geophysical Research Letters, 39, L06802, https://doi.org/10.1029/2012GL050905, 2012.

Shi, J., Hong, J., Ma, N., Luo, Q., He, Y., Xu, H., Tan, H., Wang, Q., Tao, J., Zhou, Y., Han, S., Peng, L., Xie, L., Zhou, G., Xu, W., Sun, Y., Cheng, Y., and Su, H.: Measurement report: On the difference in aerosol hygroscopicity between high and low relative humidity conditions in the North China Plain, Atmos. Chem. Phys., 22, 4599–4613, https://doi.org/10.5194/acp-22-4599-2022, 2022.

Stevens, R., Ryjkov, A., Majdzadeh, M., and Dastoor, A.: An improved representation of aerosol mixing state for air quality–weather interactions, Atmos. Chem. Phys., 22, 13527–13549, https://doi.org/10.5194/acp-22-13527-2022, 2022.

Stolzenburg, M. R. and McMurry, P. H.: Equations governing single and tandem DMA configurations and a new lognormal approximation to the transfer function, Aerosol Science and Technology, 42, 421–432, 2008.

Su, H., Rose, D., Cheng, Y. F., Gunthe, S. S., Massling, A., Stock, M., Wiedensohler, A., Andreae, M. O., and Poschl, U.: Hygroscopicity distribution concept for measurement data analysis and modeling of aerosol particle mixing state with regard to hygroscopic growth and CCN activation, Atmos. Chem. Phys., 10, 7489–7503, https://doi.org/10.5194/acp-10-7489-2010, 2010.

Subramanian, R., Kok, G. L., Baumgardner, D., Clarke, A., Shinozuka, Y., Campos, T. L., Heizer, C. G., Stephens, B. B., de Foy, B., Voss, P. B., and Zaveri, R. A.: Black carbon over Mexico: the effect of atmospheric transport on mixing state, mass absorption cross-section, and BC/CO ratios, Atmos. Chem. Phys., 10, 219–237, https://doi.org/10.5194/acp-10-219-2010, 2010.

Tan, H., Xu, H., Wan, Q., Li, F., Deng, X., Chan, P. W., Xia, D., and Yin, Y.: Design and Application of an Unattended Multifunctional H-TDMA System, Journal of Atmospheric and Oceanic Technology, 30, 1136–1148, https://doi.org/10.1175/JTECH-D-12-00129.1, 2013.

Tao, J., Zhao, C., Nan, M., and Ye, K.: Consistency and applicability of parameterization schemes for the size-resolved aerosol activation ratio based on field measurements in the North China Plain, Atmospheric Environment, 173, 316–324, 2018.

Tao, J., Kuang, Y., Ma, N., Zheng, Y., Wiedensohler, A., and Zhao, C.: An improved parameterization scheme for size-resolved particle activation ratio and its application on comparison study of particle hygroscopicity measurements between HTDMA and DMA-CCNC, Atmospheric Environment, 226, 117403, https://doi.org/10.1016/j.atmosenv.2020.117403, 2020.

Tao, J., Kuang, Y., Ma, N., Hong, J., Sun, Y., Xu, W., Zhang, Y., He, Y., Luo, Q., Xie, L., Su, H., and Cheng, Y.: Secondary aerosol formation alters CCN activity in the North China Plain, Atmos. Chem. Phys., 21, 7409–7427, https://doi.org/10.5194/acp-21-7409-2021, 2021.

Tao, M., Chen, L., Su, L., and Tao, J.: Satellite observation of regional haze pollution over the North China Plain, Journal of Geophysical Research: Atmospheres, 117, https://doi.org/10.1029/2012JD017915, 2012.

Thalman, R., de Sa, S. S., Palm, B. B., Barbosa, H. M. J., Poehlker, M. L., Alexander, M. L., Brito, J., Carbone, S., Castillo, P., Day, D. A., Kuang, C., Manzi, A., Ng, N. L., Sedlacek, A. J., Souza, R., Springston, S., Watson, T., Poehlker, C., Poeschl, U., Andreae, M. O., Artaxo, P., Jimenez, J. L., Martin, S. T., and Wang, J.: CCN activity and organic hygroscopicity of aerosols downwind of an urban region in central Amazonia: seasonal and diel variations and impact of anthropogenic emissions, Atmospheric Chemistry and Physics, 17, 11779–11801, https://doi.org/10.5194/acp-17-11779-2017, 2017.

Ting, Y., Mitchell, E. J. S., Allan, J. D., Liu, D., Spracklen, D. V., Williams, A., Jones, J. M., Lea-Langton, A. R., McFiggans, G., and Coe, H.: Mixing State of Carbonaceous Aerosols of Primary Emissions from "Improved" African Cookstoves, Environ. Sci. Technol., 52, 10134–10143, https://doi.org/10.1021/acs.est.8b00456, 2018.

Tomlin, J. M., Jankowski, K. A., Veghte, D. P., China, S., Wang, P., Fraund, M., Weis, J., Zheng, G., Wang, Y., Rivera-Adorno, F., Raveh-Rubin, S., Knopf, D. A., Wang, J., Gilles, M. K., Moffet, R. C., and Laskin, A.: Impact of dry intrusion events on the composition and mixing state of particles during the winter Aerosol and Cloud Experiment in the Eastern North Atlantic (ACE-ENA), Atmos. Chem. Phys., 21, 18123–18146, https://doi.org/10.5194/acp-21-18123-2021, 2021.

Ulbrich, I. M., Canagaratna, M. R., Zhang, Q., Worsnop, D. R., and Jimenez, J. L.: Interpretation of organic components from Positive Matrix Factorization of aerosol mass spectrometric data, Atmos. Chem. Phys., 9, 2891–2918, https://doi.org/10.5194/acp-9-2891-2009, 2009.

Wang, X., Ye, X., Chen, J., Wang, X., Yang, X., Fu, T.-M., Zhu, L., and Liu, C.: Direct links between hygroscopicity and mixing state of ambient aerosols: estimating particle hygroscopicity from their single-particle mass spectra, Atmos. Chem. Phys., 20, 6273–6290, https://doi.org/10.5194/acp-20-6273-2020, 2020.

Wang, Y., Wang, X., Kondo, Y., Kajino, M., Munger, J. W., and Hao, J.: Black carbon and its correlation with trace gases at a rural site in Beijing: Top-down constraints from ambient measurements on bottom-up emissions, Journal of Geophysical Research: Atmospheres, 116, https://doi.org/10.1029/2011JD016575, 2011.

Wang, Y., Zhang, F., Li, Z., Tan, H., Xu, H., Ren, J., Zhao, J., Du, W., and Sun, Y.: Enhanced hydrophobicity and volatility of submicron aerosols under severe emission control conditions in Beijing, Atmos. Chem. Phys., 17, 5239–5251, https://doi.org/10.5194/acp-17-5239-2017, 2017.

Wang, Y., Hu, R., Wang, Q., Li, Z., Cribb, M., Sun, Y., Song, X., Shang, Y., Wu, Y., Huang, X., and Wang, Y.: Different effects of anthropogenic emissions and aging processes on the mixing state of soot particles in the nucleation and accumulation modes, Atmos. Chem. Phys., 22, 14133–14146, https://doi.org/10.5194/acp-22-14133-2022, 2022.

Wehner, B., Berghof, M., Cheng, Y. F., Achtert, P., Birmili, W., Nowak, A., Wiedensohler, A., Garland, R. M., Pöschl, U., Hu, M., and Zhu, T.: Mixing state of nonvolatile aerosol particle fractions and comparison with light absorption in the polluted Beijing region, Journal of Geophysical Research: Atmospheres, 114, https://doi.org/10.1029/2008JD010923, 2009.

Wu, Y., Wang, X., Tao, J., Huang, R., Tian, P., Cao, J., Zhang, L., Ho, K.-F., Han, Z., and Zhang, R.: Size distribution and source of black carbon aerosol in urban Beijing during winter haze episodes, Atmos. Chem. Phys., 17, 7965–7975, https://doi.org/10.5194/acp-17-7965-2017, 2017.

Xu, W., Sun, Y., Wang, Q., Zhao, J., Wang, J., Ge, X., Xie, C., Zhou, W., Du, W., Li, J., Fu, P., Wang, Z., Worsnop, D. R., and Coe, H.: Changes in Aerosol Chemistry From 2014 to 2016 in Winter in Beijing: Insights From High-Resolution Aerosol Mass Spectrometry, Journal of Geophysical Research: Atmospheres, 124, 1132–1147, https://doi.org/10.1029/2018JD029245, 2019.

Xu, W. Y., Zhao, C. S., Ran, L., Deng, Z. Z., Liu, P. F., Ma, N., Lin, W. L., Xu, X. B., Yan, P., He, X., Yu, J., Liang, W. D., and Chen, L. L.: Characteristics of pollutants and their correlation to meteorological conditions at a suburban site in the North China Plain, Atmos. Chem. Phys., 11, 4353–4369, https://doi.org/10.5194/acp-11-4353-2011, 2011.

Yang, Z., Ma, N., Wang, Q., Li, G., Pan, X., Dong, W., Zhu, S., Zhang, S., Gao, W., He, Y., Xie, L., Zhang, Y., Kuhn, U., Xu, W., Kuang, Y., Tao, J., Hong, J., Zhou, G., Sun, Y., Su, H., and Cheng, Y.: Characteristics and source apportionment of black carbon aerosol in the North China Plain, Atmospheric Research, 276, 106246, https://doi.org/10.1016/j.atmosres.2022.106246, 2022.

Zhang, F., Li, Y., Li, Z., Sun, L., Li, R., Zhao, C., Wang, P., Sun, Y., Liu, X., Li, J., Li, P., Ren, G., and Fan, T.: Aerosol hygroscopicity and cloud condensation nuclei activity during the AC3Exp campaign: implications for cloud condensation nuclei parameterization, Atmos. Chem. Phys., 14, 13423–13437, https://doi.org/10.5194/acp-14-13423-2014, 2014.

Zhang, S., Shen, X., Sun, J., Zhang, Y., Zhang, X., Xia, C., Hu, X., Zhong, J., Wang, J., and Liu, S.: Atmospheric Particle Hygroscopicity and the Influence by Oxidation State of Organic Aerosols in Urban Beijing, Journal of Environmental Sciences, 124, 544–556, https://doi.org/10.1016/j.jes.2021.11.019, 2023.

Zhang, S. L., Ma, N., Kecorius, S., Wang, P. C., Hu, M., Wang, Z. B., Größ, J., Wu, Z. J., and Wiedensohler, A.: Mixing state of atmospheric particles over the North China Plain, Atmospheric Environment, 125, 152–164, 2016.

Zhang, Y., Su, H., Ma, N., Li, G., Kecorius, S., Wang, Z., Hu, M., Zhu, T., He, K., Wiedensohler, A., Zhang, Q., and Cheng, Y.: Sizing of Ambient Particles From a Single-Particle Soot Photometer Measurement to Retrieve Mixing State of Black Carbon at a Regional Site of the North China Plain, Journal of Geophysical Research: Atmospheres, 123, 12,778-12,795, https://doi.org/10.1029/2018JD028810, 2018.

Zhao, G., Tao, J., Kuang, Y., Shen, C., Yu, Y., and Zhao, C.: Role of black carbon mass size distribution in the direct aerosol radiative forcing, Atmos. Chem. Phys., 19, 13175–13188, https://doi.org/10.5194/acp-19-13175-2019, 2019.

Zhao, G., Tan, T., Hu, S., Du, Z., Shang, D., Wu, Z., Guo, S., Zheng, J., Zhu, W., Li, M., Zeng, L., and Hu, M.: Mixing state of black carbon at different atmospheres in north and southwest China, Atmos. Chem. Phys., 22, 10861–10873, https://doi.org/10.5194/acp-22-10861-2022, 2022.

Zheng, H., Kong, S., Wu, F., Cheng, Y., Niu, Z., Zheng, S., Yang, G., Yao, L., Yan, Q., Wu, J., Zheng, M., Chen, N., Xu, K., Yan, Y., Liu, D., Zhao, D., Zhao, T., Bai, Y., Li, S., and Qi, S.: Intra-regional transport of black carbon between the south edge of the North China Plain and central China during winter haze episodes, Atmos. Chem. Phys., 19, 4499–4516, https://doi.org/10.5194/acp-19-4499-2019, 2019.

Zhuang, B. L., Li, S., Wang, T. J., Deng, J. J., Xie, M., Yin, C. Q., and Zhu, J. L.: Direct radiative forcing and climate effects of anthropogenic aerosols with different mixing states over China, Atmospheric Environment, 79, 349–361, https://doi.org/10.1016/j.atmosenv.2013.07.004, 2013.

Table 1. Definition and description of abbreviations.

Abbreviation	Full name and/or Definition
BBOA	Biomass Burning Organic Aerosol Characterized by obvious m/z 60 (mainly $C_2H_4O_2^+$) and 73 (mainly $C_3H_5O_2^+$), which are two indicators of biomass burning
FFOA	Fossil Fuel Organic Aerosol A mixed factor that comprises traffic emissions and coal combustion, which was characterized by typical hydrocarbon ion series
OOA	Oxygenated Organic Aerosol
OOA1 and OOA2	Two OOA factors resolved from the PMF analysis
SOA	Secondary Organic Aerosol Summation of OOA1 and OOA2
POA	Primary Organic Aerosol Summation of BBOA and FFOA
SIA	Secondary Inorganic Aerosols, including nitrate, sulfate, and ammonium
$PM_{2.5}$	Particulate Matter with an aerodynamic diameter <2.5 μm
PM_1	Particulate Matter with an aerodynamic diameter <1 μm
NR-PM_1	Non-refractory PM_1
MF	Mass Fraction
D_p	Particle diameter after humidification or heating
D_d	Particle diameter under dry conditions without humidification or heating
κ	Hygroscopicity parameter
SS	Supersaturation
SPAR	Size-resolved Particle Activation Ratio

	Size-dependent CCN activity under a specific SS
MAF	Maximum Activation Fraction An asymptote of the measured SPAR curve at large particle sizes and represents the number fraction of CCNs to total particles
D_a	Midpoint activation diameter Linked to the hygroscopicity of CCNs
GF	Growth factor The ratio between particles with and without humidification and is linked to aerosol hygroscopicity
SF	Shrinkage Factor The ratio between particles with and without heating and is linked to aerosol volatility
PDF	Probability Distribution Function
NF_H	Number Fraction of Hydrophilic aerosol whose hygroscopicity parameter is >~0.07
NF_V	Number Fraction of Volatile aerosol whose Shrinkage Factor at 200 °C is <0.85
NF_{noBC}	Number Fraction of black carbon (BC)-free particles
NF_{CBC}	Number Fraction of thickly coated BC particles
R_{exBC}	The number concentration ratio of externally mixed BC particles in total BC-containing particles Externally mixed BC particles are defined as identified bare/thinly coated BC-containing particles
NF_A-NF_B (NF_{noBC}-NF_H, NF_V-NF_H, NF_{noBC}-NF_V, NF_V-MAF, NF_{noBC}-MAF)	The difference between the number fraction of A and B

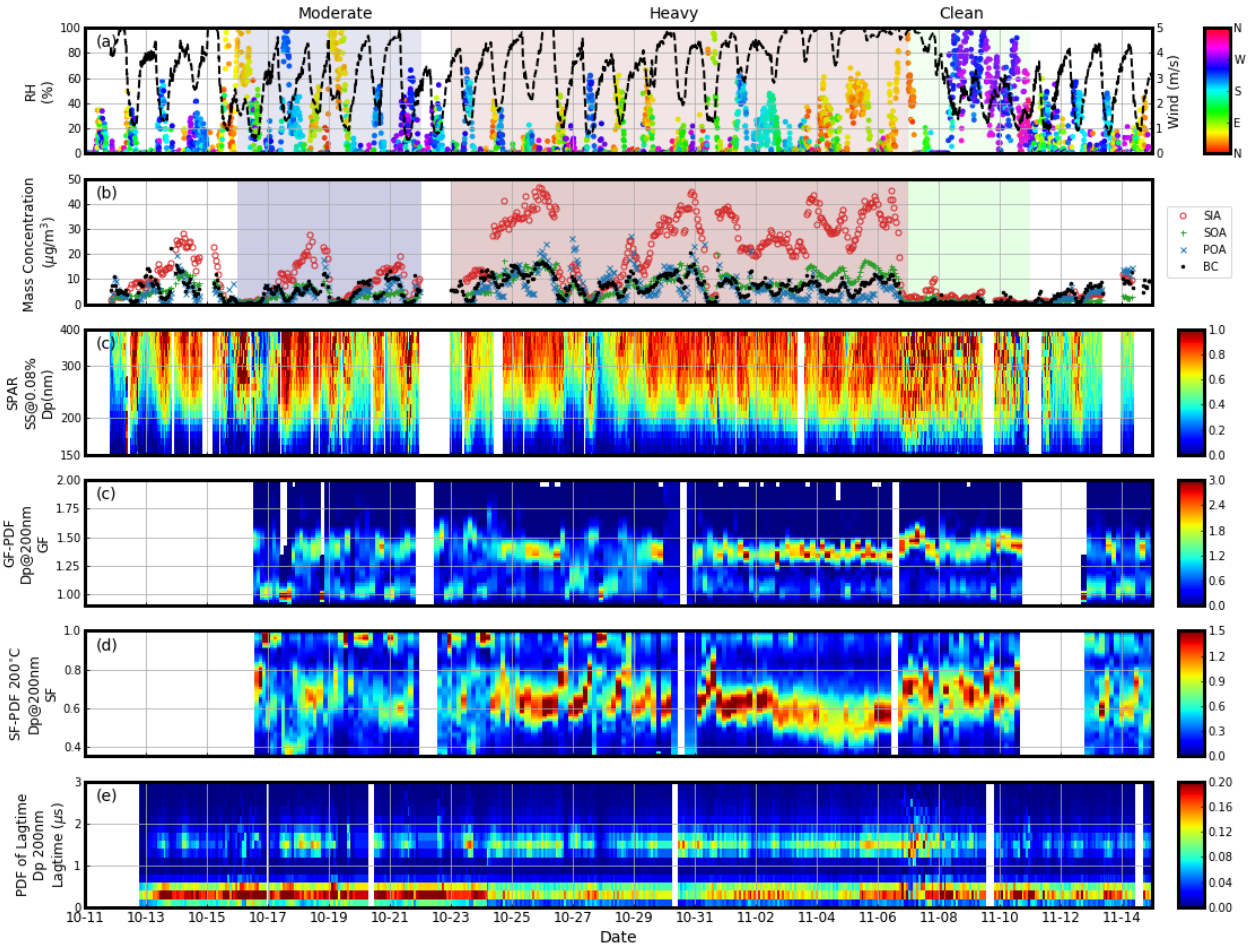
Moderate
Heavy
Clean
(a)
RH (%)
Wind (m/s)
N
W
S
E
N
(b)
Mass Concentration (μg/m³)
SIA
SOA
POA
BC
(c)
SPAR SS@0.08% Dp(nm)
(c)
GF-PDF Dp@200nm GF
(d)
SF-PDF 200°C Dp@200nm SF
(e)
PDF of Lagtime Dp 200nm Lagtime (μs)
10-11
10-13
10-15
10-17
10-19
10-21
10-23
10-25
10-27
10-29
10-31
11-02
11-04
11-06
11-08
11-10
11-12
11-14
Date

1104

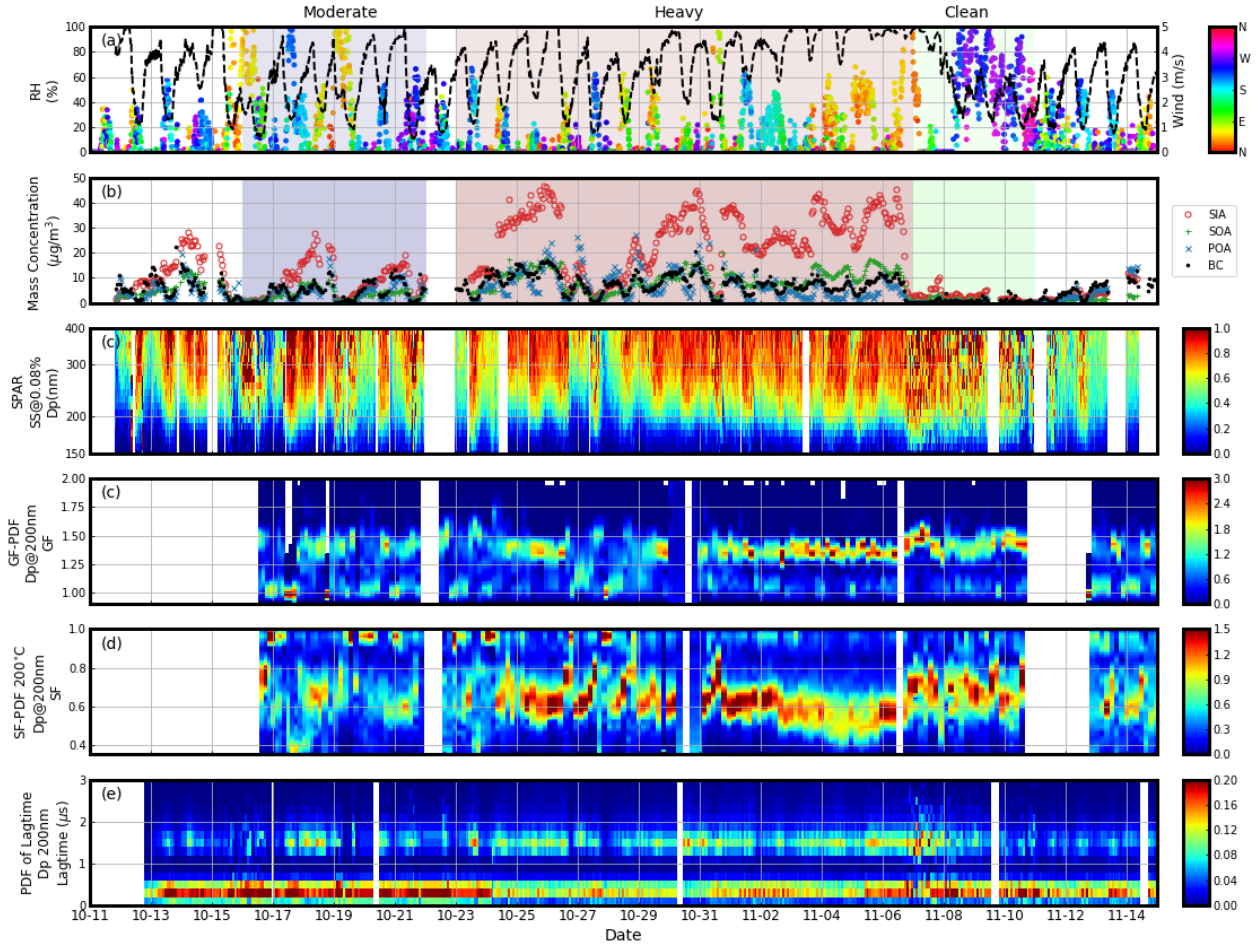

~~Fig~~**Figure 1**. Overview of the measurements during the campaign: **(a)** ~~dots represent~~meteorological parameters: wind speed ~~with color indicating~~(dots) and relative humidity (RH) (black line), with colors of dots representing wind direction~~, and black lines represent RH~~; **(b)** mass concentrations of aerosol chemical compositions: secondary inorganic aerosols (SIA, red circle), secondary organic aerosols (SOA, green plus), primary organic aerosols (POA, blue x) and black carbon (BC, black dots ~~represent mass concentration of SIA, SOA, POA and BC, respectively;~~); **(c)** Size-resolved Particle Activation Ratio (SPAR) under supersaturation (SS) of 0.08~~%~~;% observed by the DMA-CCNC, with warmer colors corresponding to higher values; **(d)** ~~PDF of GF (GFPDF) at 200 nm; (e)~~ Probability Density Function (PDF) of ~~SF (SFPDF~~growth factor (GF-PDF) at 200- nm observed by the HTDMA; **(e)** PDF of shrinkage factor (SF-PDF) at 200 nm and 200-~~°C~~ °C observed by the VTDMA; **(f)** PDF of lag- time at 200- nm~~.~~ observed by the DMA-SP2. The blue, red, and green shaded periods represent the three periods with moderate pollution, heavy pollution, and clean ~~condition~~conditions, respectively.

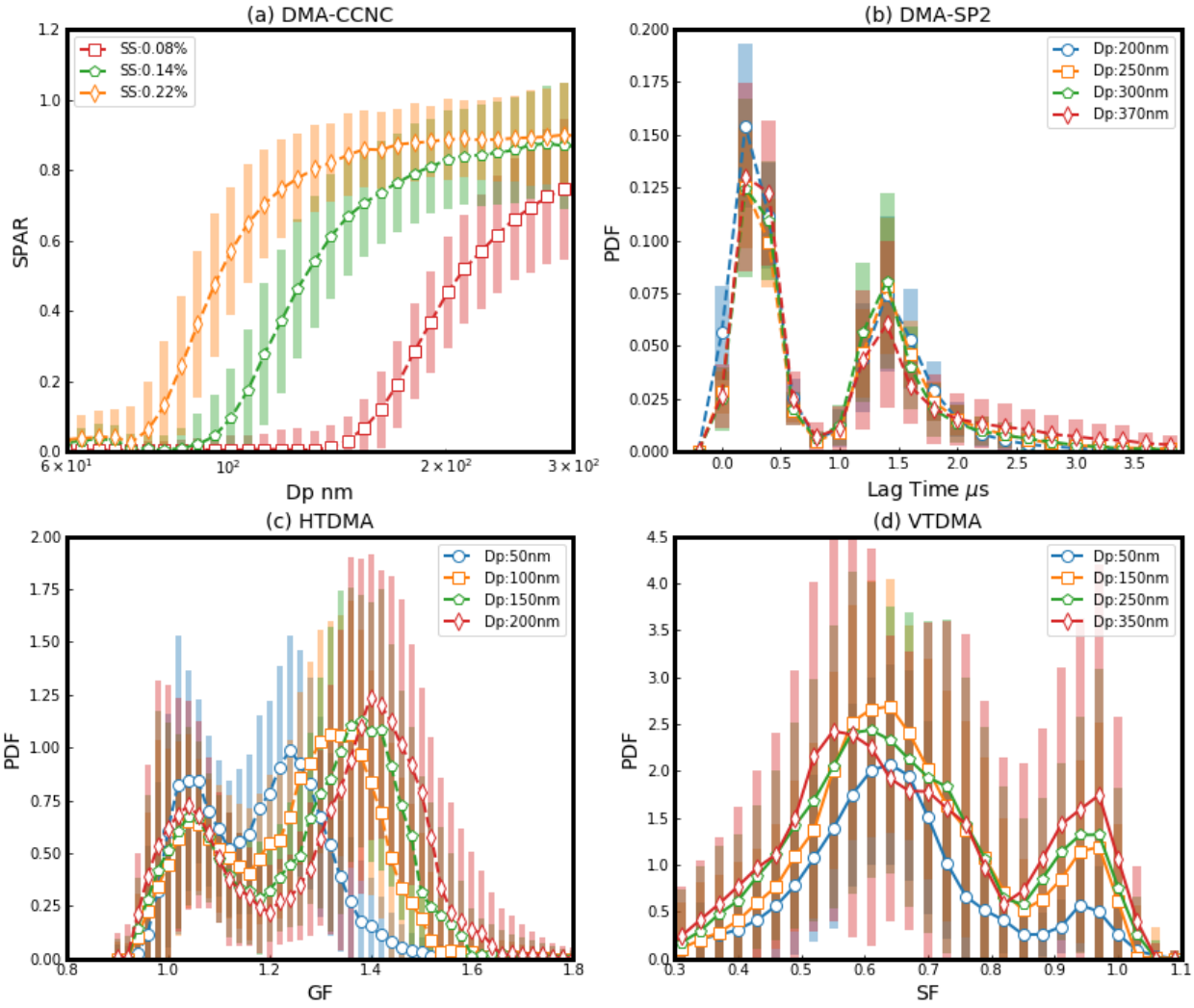
(a) DMA-CCNC
SS:0.08%
SS:0.14%
SS:0.22%
SPAR
Dp nm
(b) DMA-SP2
Dp:200nm
Dp:250nm
Dp:300nm
Dp:370nm
PDF
Lag Time μs
(c) HTDMA
Dp:50nm
Dp:100nm
Dp:150nm
Dp:200nm
PDF
GF
(d) VTDMA
Dp:50nm
Dp:150nm
Dp:250nm
Dp:350nm
PDF
SF

1117

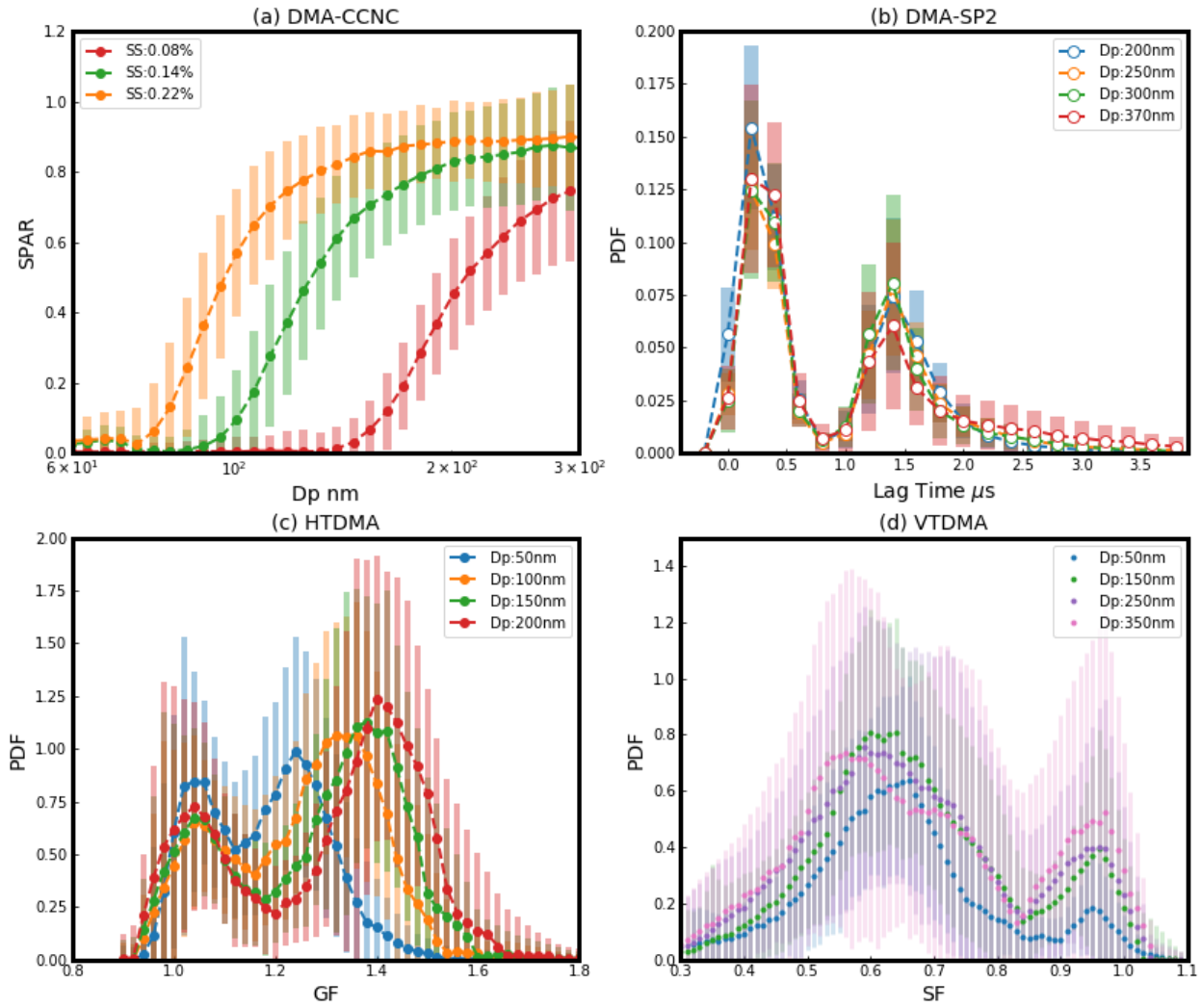

~~Fig.~~**Figure 2**. The campaign average of **(a)** ~~SPAR~~Size-resolved Particle Activation Ratio (SPAR) curves measured by DMA-CCNC at the three supersaturations (SSs ~~(identified,~~ represented by different colors and markers), **(b)** Probability Density Function (PDF) of lag- time measured by DMA-SP2 at four particle sizes (~~identified~~represented by different colors and markers), **(c)** PDF of growth factor (GF ~~(GFPDF)~~) measured by HTDMA at four particle sizes (~~identified~~represented by different colors and markers), **(d)** PDF of ~~SF (SFPDF~~shrinkage factor (SF) measured by VTDMA under the temperature of 200 °C at five particle sizes (~~identified~~represented by different colors and markers). The shaded areas indicate the standard deviations.

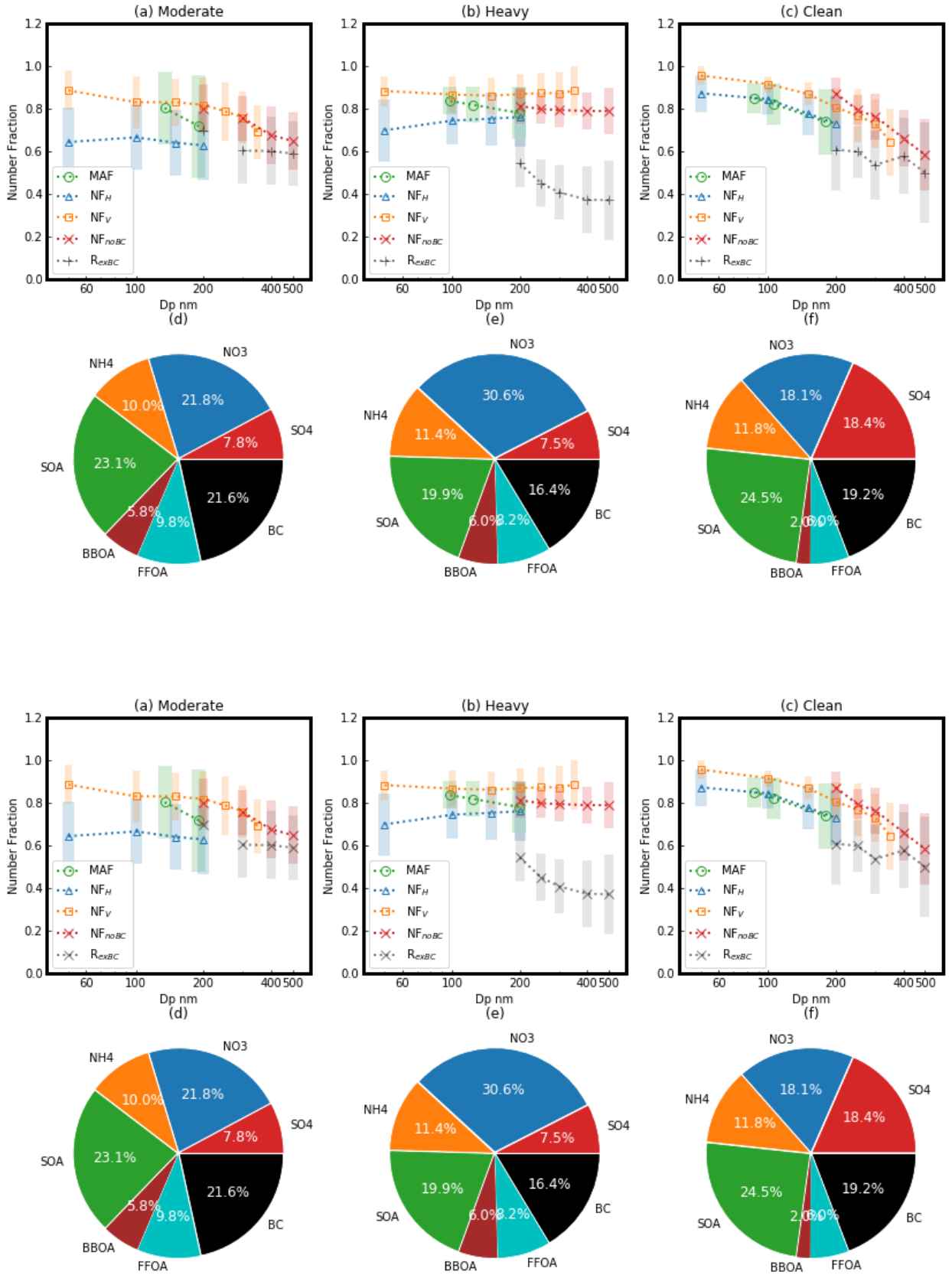

(a) Moderate
(b) Heavy
(c) Clean
Number Fraction
Dp nm
MAF
NF_H
NF_V
NF_noBC
R_exBC
(d)
(e)
(f)
NO3
NH4
SO4
SOA
BC
BBOA
FFOA
21.8%
10.0%
7.8%
23.1%
21.6%
5.8%
9.8%
30.6%
11.4%
7.5%
19.9%
16.4%
6.0%
8.2%
18.1%
11.8%
18.4%
24.5%
19.2%

Fig. **Figure 3**. **(a – c).)** Size dependence of MAF (green circle), NF_H (blue triangle), NF_V at 200 °C (yellow square-),

NF_{noBC} (red x~~)~~), and R_{exBC} (black ~~plus~~x) during the three periods. **MAF**: Maximum Activation Fraction, an asymptote of the measured Size-resolved Particle Activation Ratio (SPAR) curve at large particle. **NF_H**: Number Fraction of Hydrophilic aerosol whose hygroscopicity parameter is higher than ~0.07. **NF_V**: Number Fraction of Volatile aerosol whose Shrink Factor at 200 °C is lower than 0.85. **NF_{noBC}**: Number Fraction of black carbon (BC)-free particles. **R_{exBC}**: Number fraction of externally mixed BC particles in total BC-containing particles. **(d ~~–~~ f~~).~~)** Corresponding mass fractions (MFs) of aerosol chemical compositions (identified by colors) during the three periods~~.~~, including secondary organic aerosols (SOA), biomass burning organic aerosol (BBOA), fossil fuel organic aerosols (FFOA), and inorganic ions including sulfate (SO_4), nitrate (NO_3), and ammonium (NH_4).

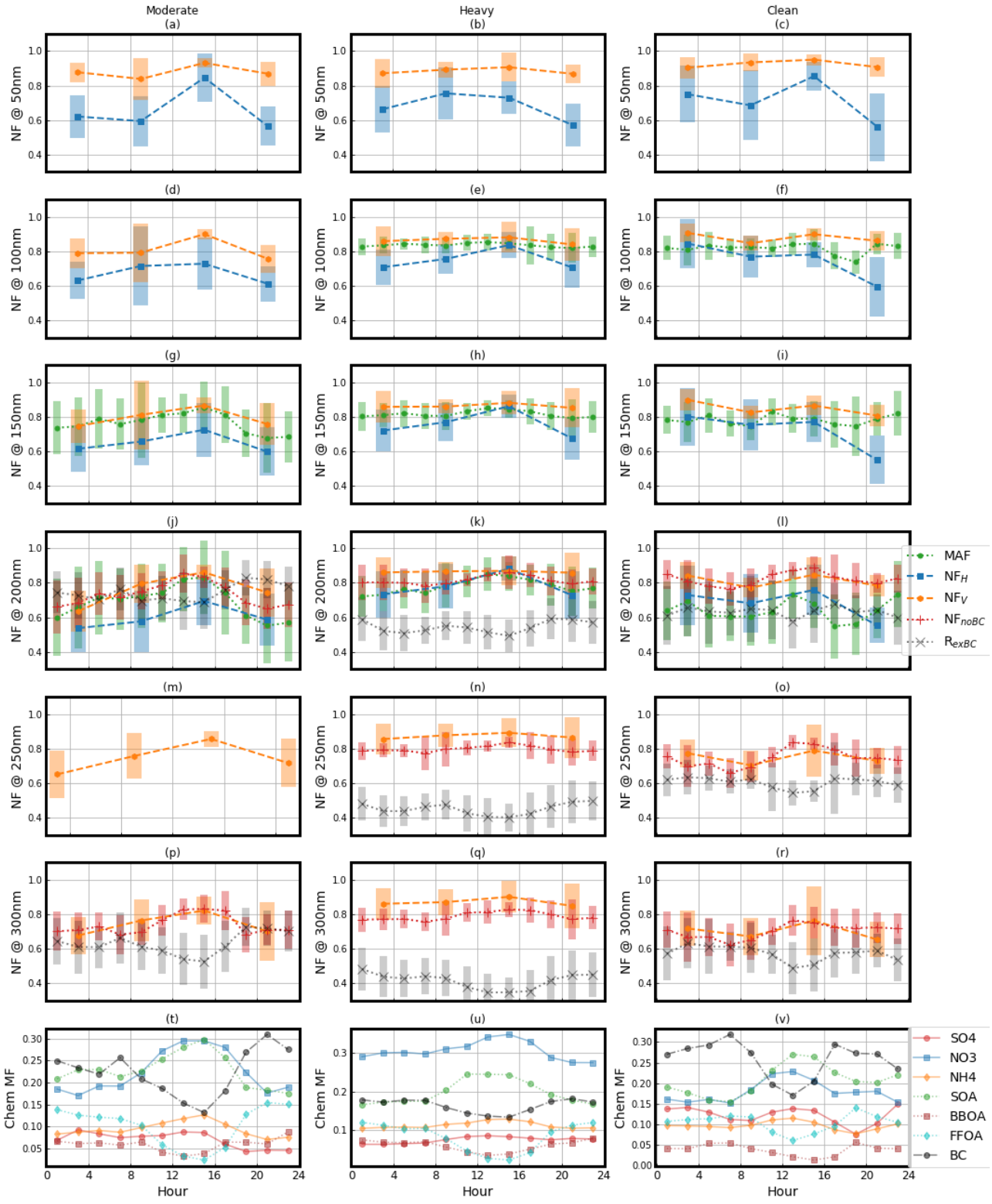
Moderate
Heavy
Clean
(a)
(b)
(c)
(d)
(e)
(f)
(g)
(h)
(i)
(j)
(k)
(l)
(m)
(n)
(o)
(p)
(q)
(r)
(t)
(u)
(v)
NF @ 50nm
NF @ 100nm
NF @ 150nm
NF @ 200nm
NF @ 250nm
NF @ 300nm
Chem MF
Hour
MAF
NF_H
NF_V
NF_{noBC}
R_{exBC}
SO4
NO3
NH4
SOA
BBOA
FFOA
BC

1137

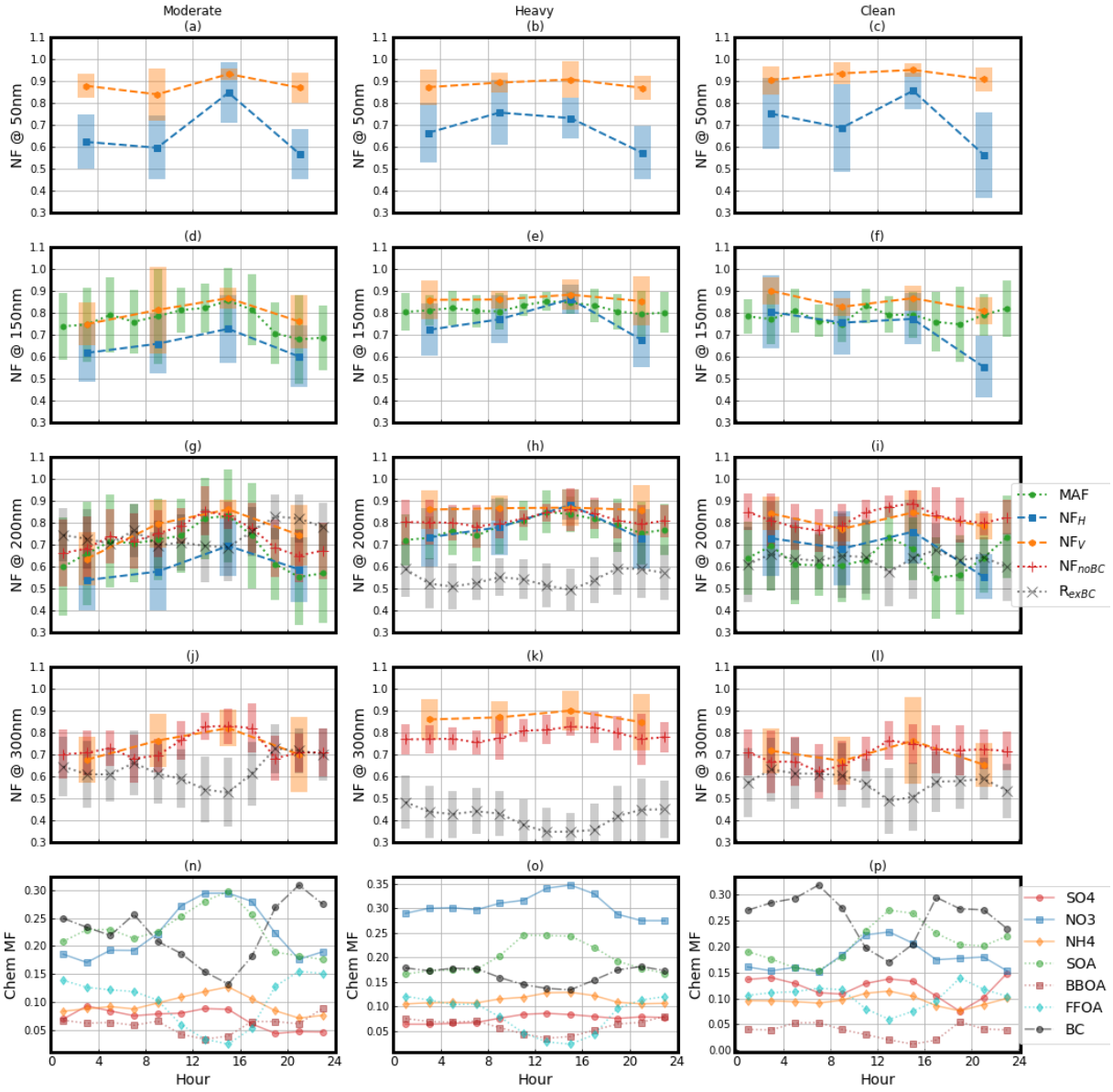

Fig.**Figure 4. (a**–r–l**)** Diurnal ~~variation~~variations of aerosol mixing state parameters (identified by color and marker) at different particle ~~size~~ sizes (50, 150, 200, and 300 nm) during the three periods. ~~(t–v~~The shaded areas indicate the standard deviations. **(m–o)** Diurnal ~~variation~~variations of mass ~~fraction of aerosol chemical compositions~~fractions (MFs) of aerosol chemical compositions, including secondary organic aerosols (SOA), biomass burning organic aerosol (BBOA), fossil fuel organic aerosols (FFOA), and inorganic ions including sulfate (SO_4), nitrate (NO_3), and ammonium (NH_4) (identified by color and marker) during the three periods.

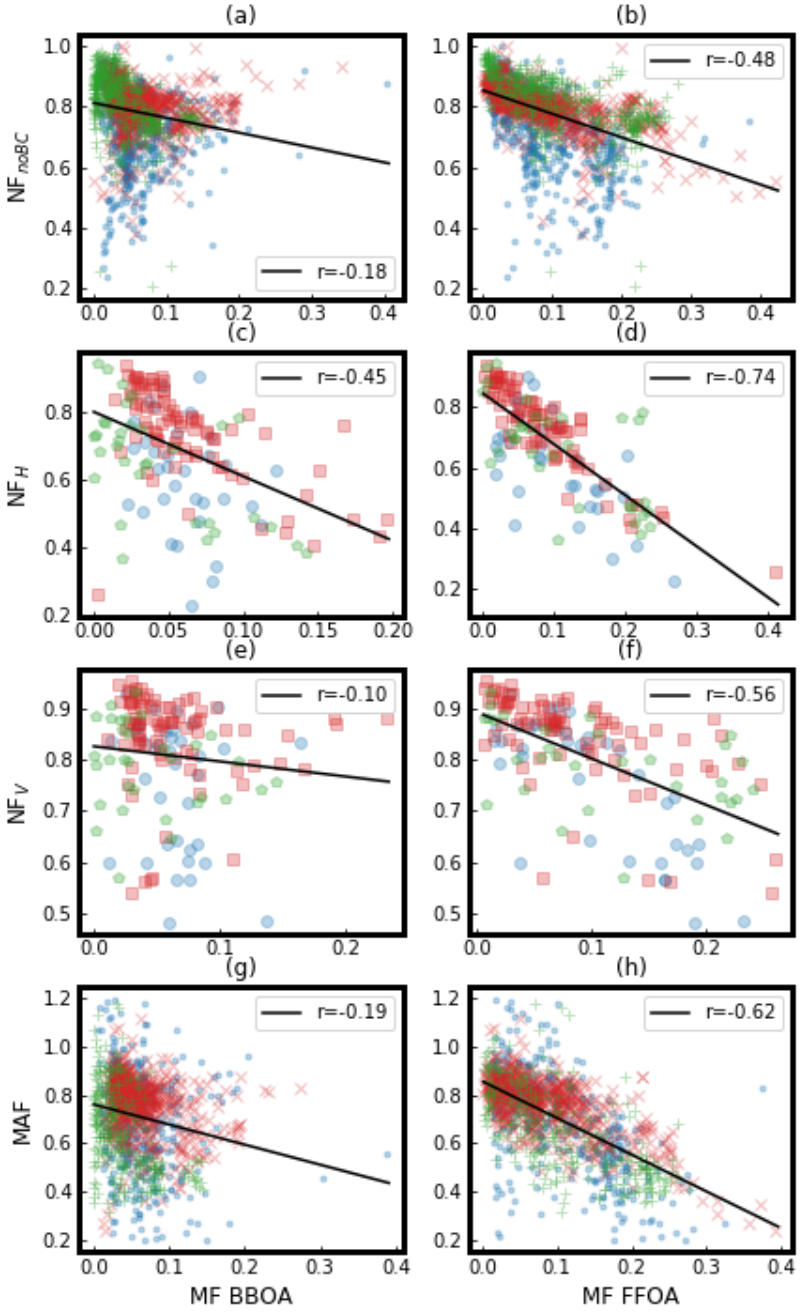
(a)
(b)
(c)
(d)
(e)
(f)
(g)
(h)
r=-0.18
r=-0.48
r=-0.45
r=-0.74
r=-0.10
r=-0.56
r=-0.19
r=-0.62
NF noBC
NF H
NF V
MAF
MF BBOA
MF FFOA

1146

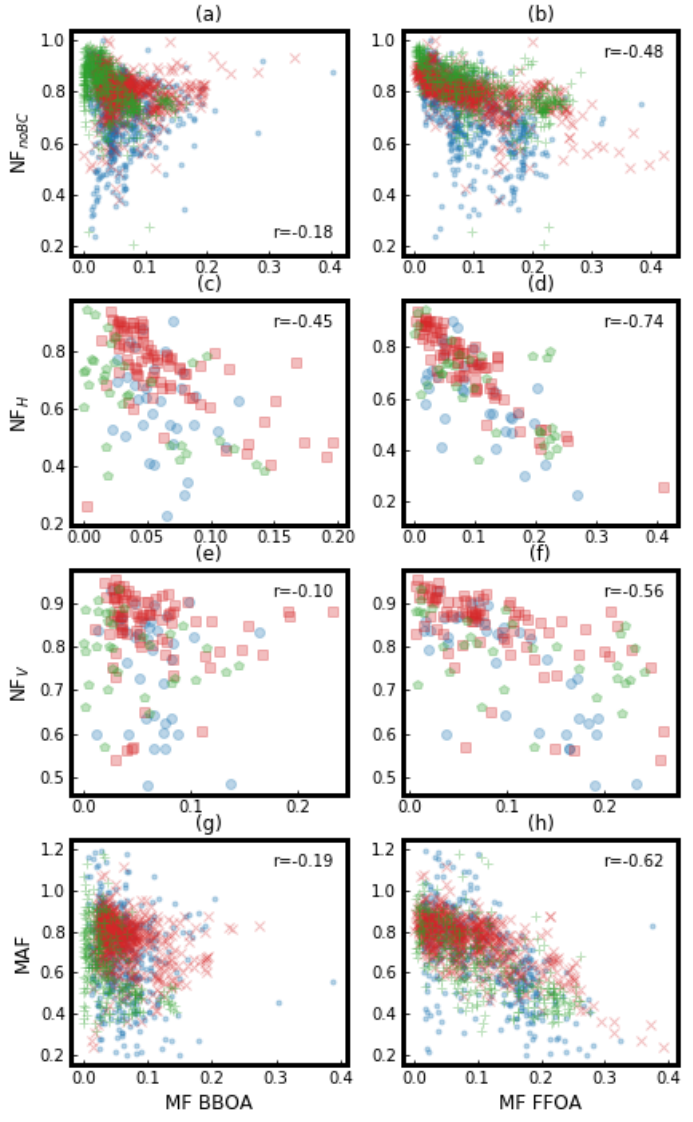

Fig.**Figure 5**. The correlationcorrelations between aerosol mixing state parameters and MFmass fractions (MFs) of primarybiomass burning organic aerosol chemical compositionBBOA) and fossil fuel organic aerosols (FFOA) during different periods. Moderately (moderately polluted period: Blueblue dot or circle; Heavilyheavily polluted period: Redred x or square; Cleanclean period: Greengreen plus or pentagon.), with r representing the correlation coefficient.

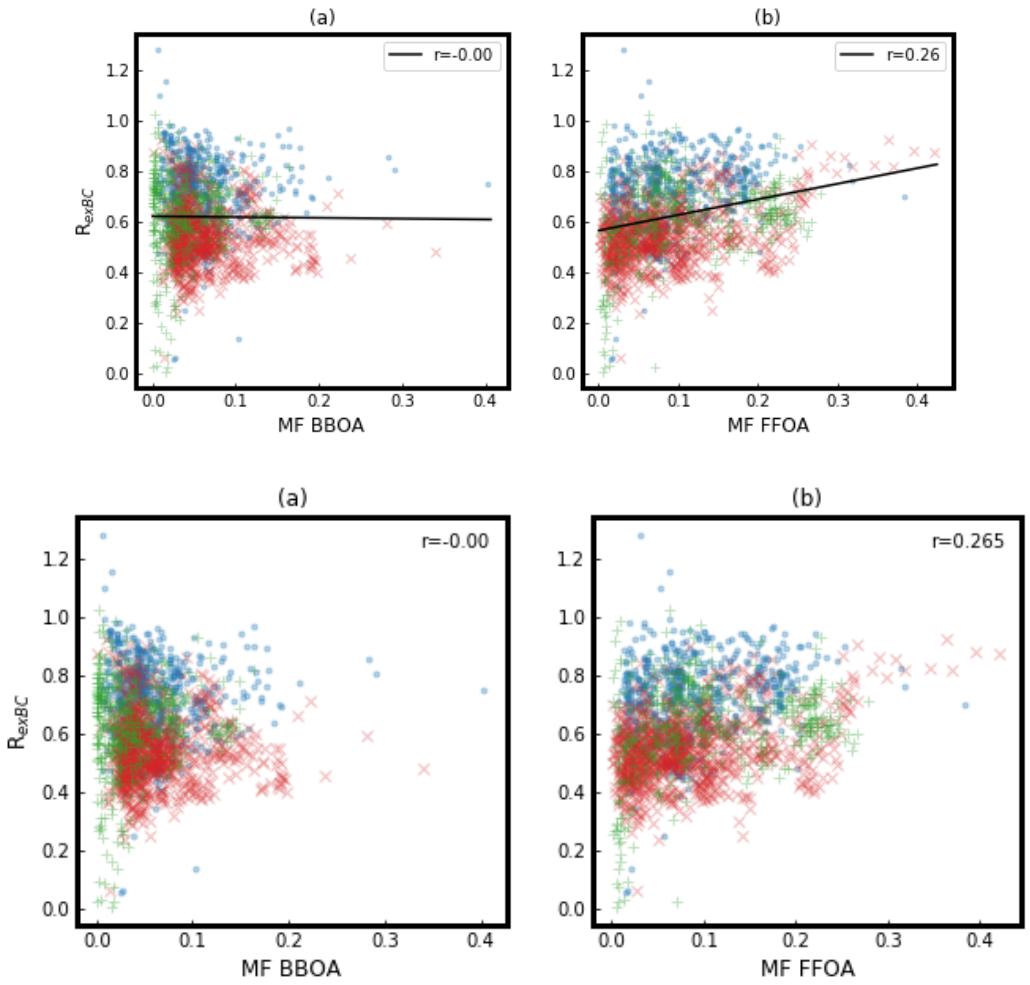

~~Fig.~~**Figure 6**. The ~~correlation~~correlations between the ratio of ~~external~~externally mixed black carbon (BC) in total BC particles ($\mathbf{R_{exBC}}$) and ~~MF~~mass fractions (MFs) of ~~primary~~biomass-burning organic aerosol ~~chemical composition~~(**BBOA**) and fossil fuel organic aerosols (**FFOA**) during different periods~~. Moderately~~ (moderately polluted period: ~~Blue~~blue dot; ~~Heavily~~heavily polluted period: ~~Red~~red x; ~~Clean~~clean period: ~~Green~~green plus~~.~~), with r representing correlation coefficient.

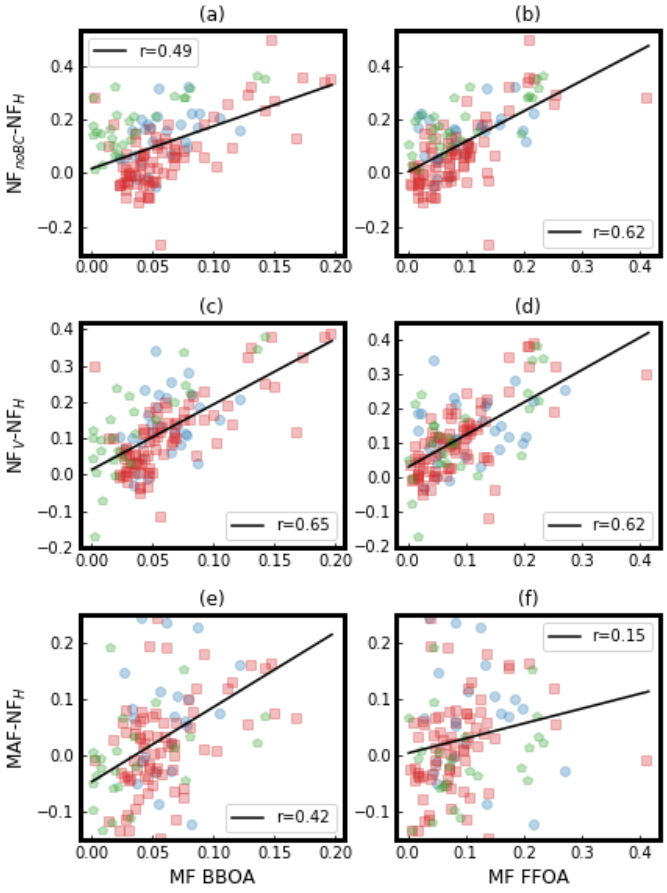

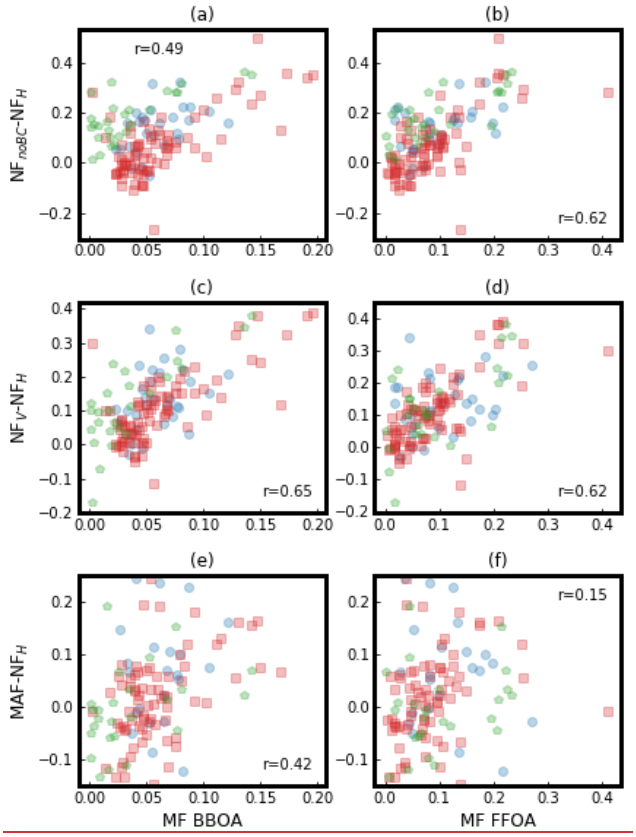

Fig. **Figure 7**. The correlation correlations between the difference among the four aerosol mixing state parameters at

particle size 200 nm and ~~MF~~mass fractions (MFs) of ~~primary~~biomass burning organic aerosol ~~chemical composition~~(**BBOA**) and fossil fuel organic aerosols (**FFOA**) during different periods~~. Moderately~~ (moderately polluted period: ~~Blue~~blue circle; ~~Heavily~~heavily polluted period: ~~Red~~red square; ~~Clean~~clean period: ~~Green~~green pentagon~~.~~), with r representing correlation coefficient.

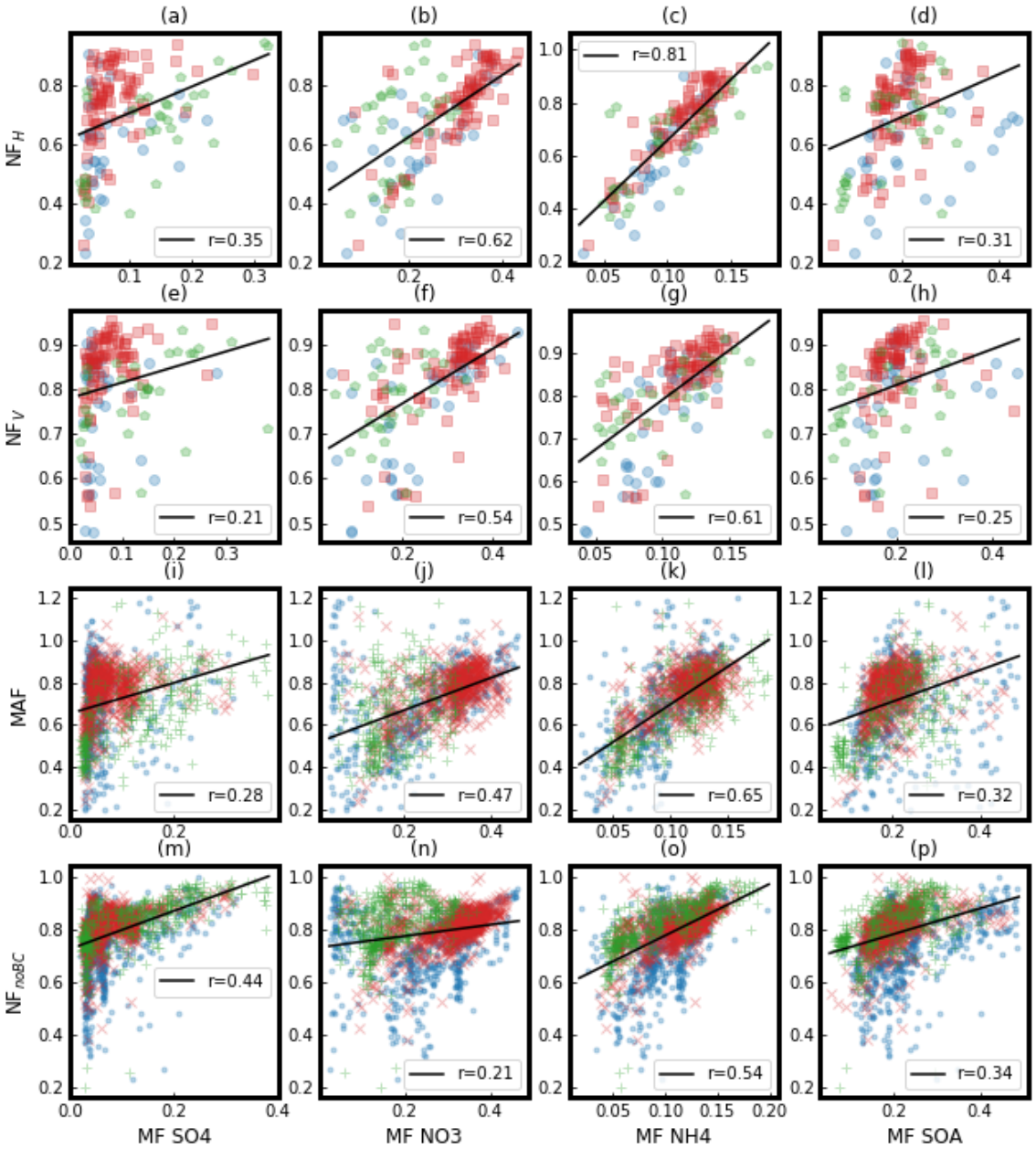
(a)
(b)
(c)
(d)
(e)
(f)
(g)
(h)
(i)
(j)
(k)
(l)
(m)
(n)
(o)
(p)
NF_H
NF_V
MAF
NF_noBC
r=0.35
r=0.62
r=0.81
r=0.31
r=0.21
r=0.54
r=0.61
r=0.25
r=0.28
r=0.47
r=0.65
r=0.32
r=0.44
r=0.21
r=0.54
r=0.34
MF SO4
MF NO3
MF NH4
MF SOA

1167

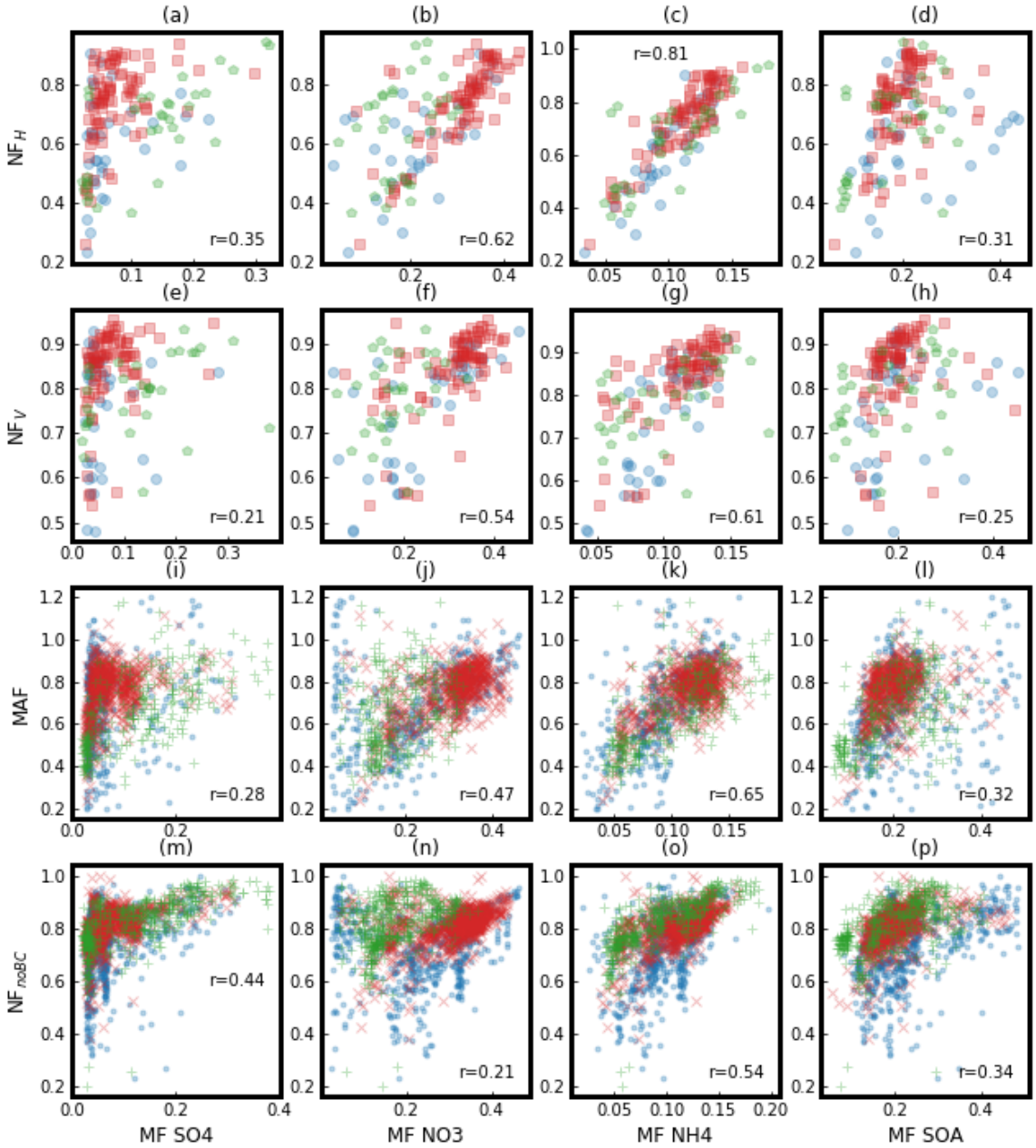

~~Fig.~~**Figure 8**. The correlation between the four aerosol mixing state parameters and mass fraction (MF) of secondary aerosol ~~chemical composition~~(SA) components during different periods~~. Moderately~~ (moderately polluted period: ~~Blue~~blue dot or circle; ~~Heavily~~heavily polluted period: ~~Red~~red x or square; ~~Clean~~clean period: ~~Green~~green plus or pentagon~~.~~), with r representing correlation coefficient. SA components include secondary organic aerosols (SOA), sulfate (SO_4), nitrate (NO_3), and ammonium (NH_4)

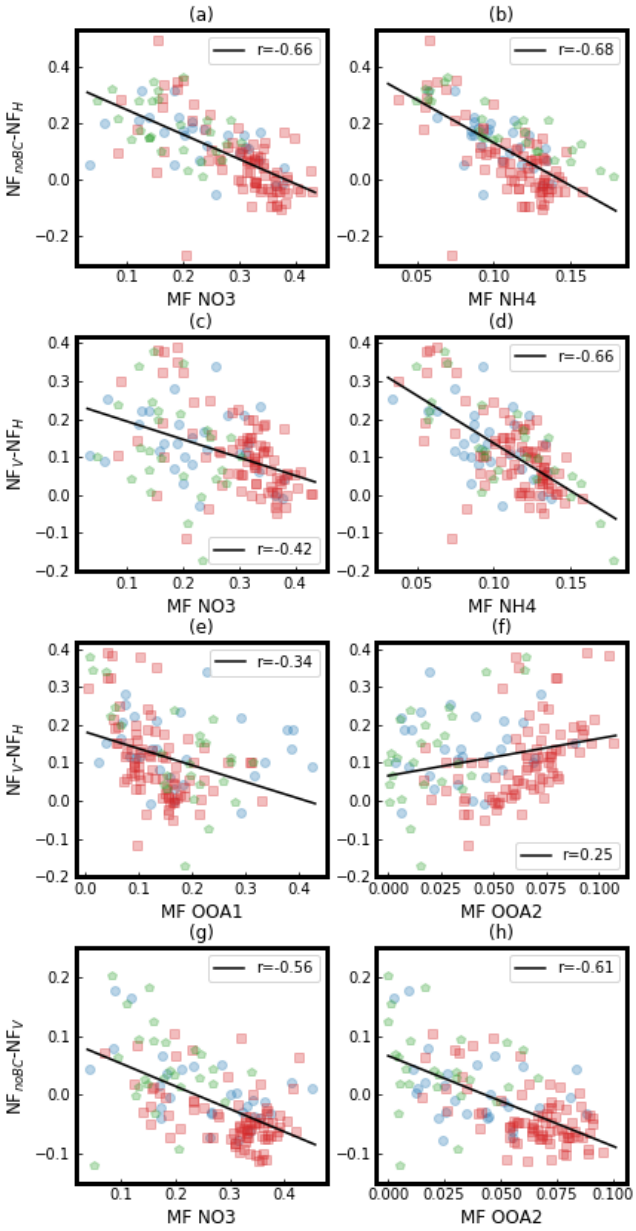
(a)
r=-0.66
NF_{noBC}-NF_H
MF NO3
(b)
r=-0.68
MF NH4
(c)
r=-0.42
NF_V-NF_H
MF NO3
(d)
r=-0.66
MF NH4
(e)
r=-0.34
NF_V-NF_H
MF OOA1
(f)
r=0.25
MF OOA2
(g)
r=-0.56
NF_{noBC}-NF_V
MF NO3
(h)
r=-0.61
MF OOA2

1174

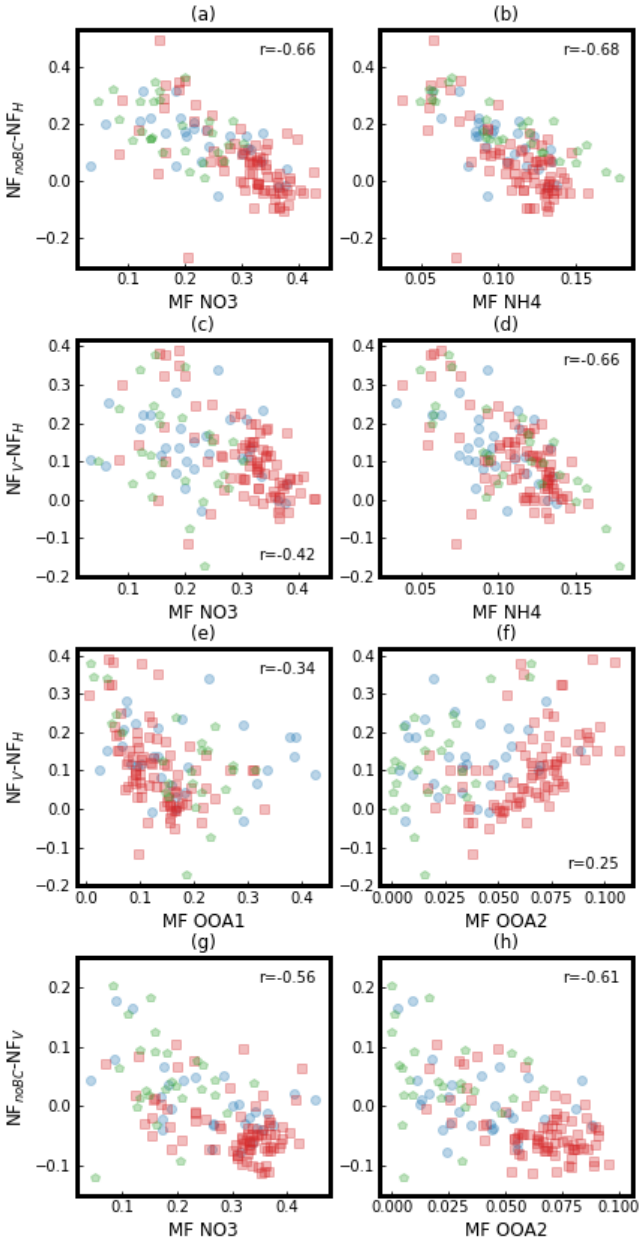

Fig. **Figure 9**. The correlation between the difference among the four aerosol mixing state parameters and mass fraction (MF) of secondary aerosol (SA) chemical compositioncomponents during different periods. OOA1 and OOA2 are two secondary organic aerosol (SOA) factors resolved from aerosol mass spectrometer (AMS) measurements using the Positive Matrix Factorization (PMF) technique. Moderately polluted period: Blueblue circle; Heavilyheavily polluted period: Redred square; Cleanclean period: Greengreen pentagon.

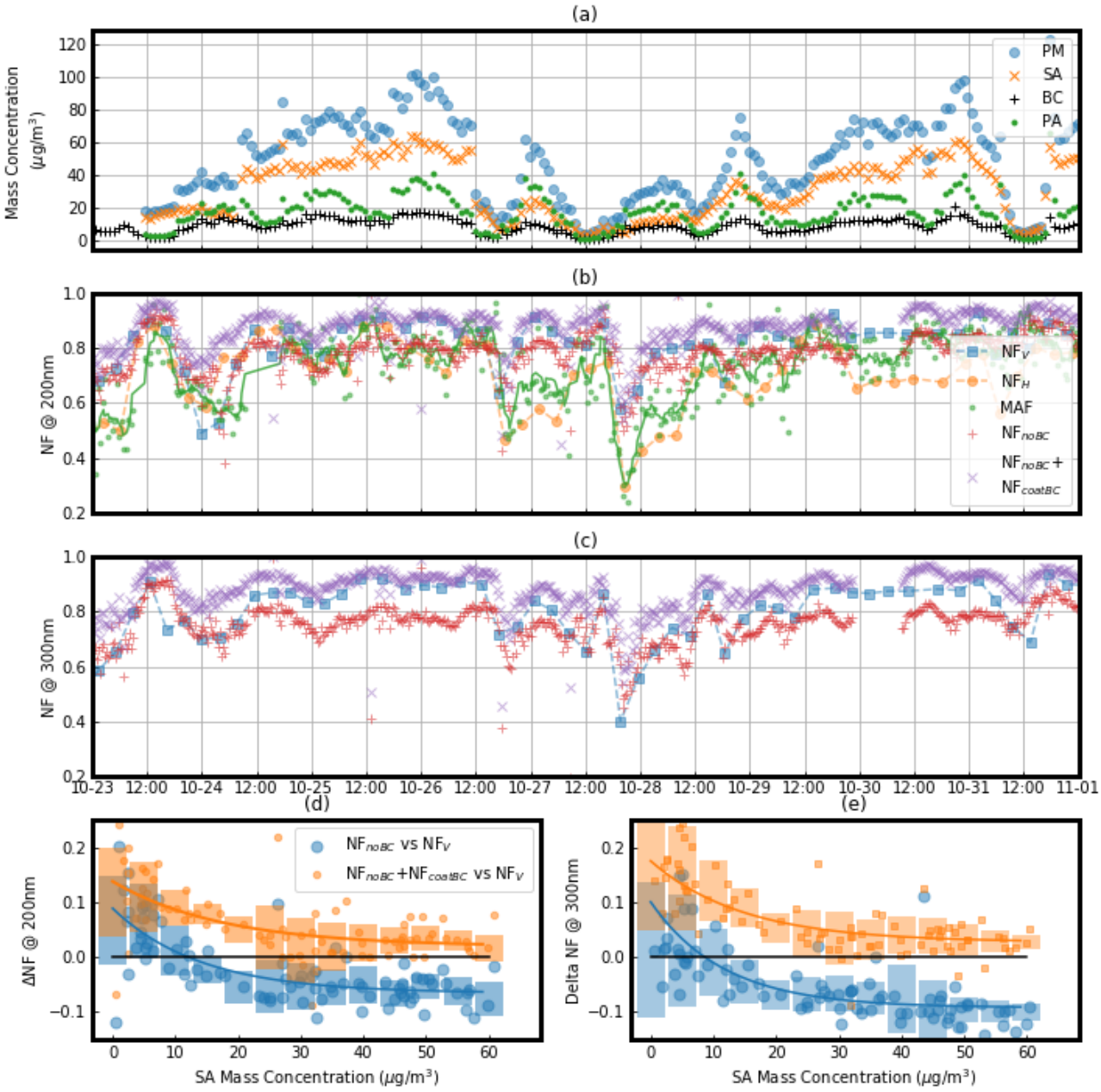

Fig. 10. The variations of different aerosol mixing state parameters during the pollution accumulation process. (a) The mass concentration of PM, SA, PA and BC (identified by colors and markers). (b and c) The variations of different aerosol mixing state parameters (identified by colors and markers) at particle size of 200nm (b) and 300nm (c); (d and e) The variations of the difference between NFV-NFnoBC (blue large circle) and NFV-NFnoBC+CBC (yellow small circle) with the mass concentration of SA at particle size of 200nm (d) and 300nm (e).

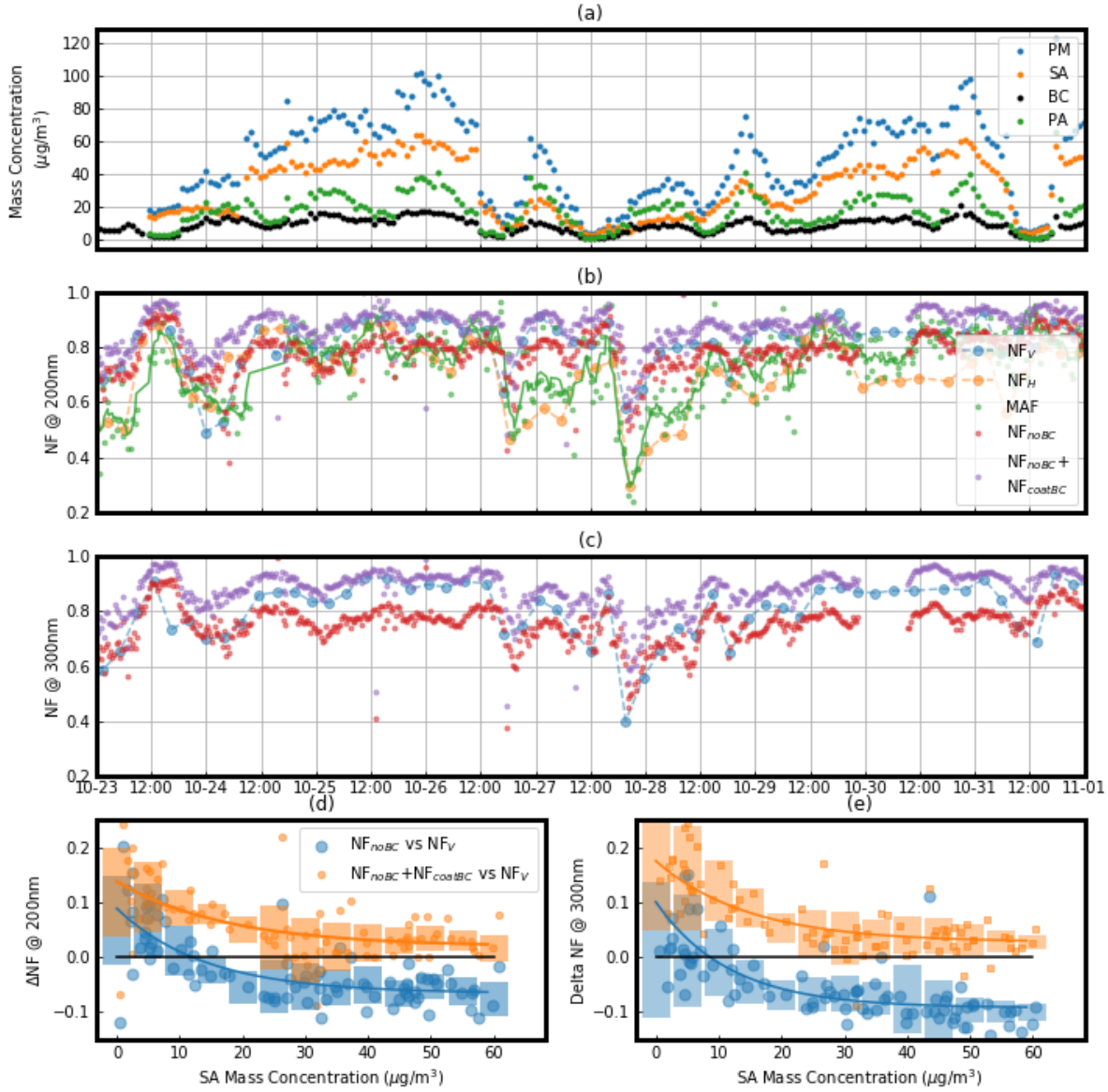

Figure 10. Variations of different aerosol mixing state parameters during the pollution accumulation process. **(a)** The time series of mass concentrations of non-refractory PM_1 (NR-PM_1), secondary aerosols (SAs) (including inorganic ions and secondary organic aerosols (SOA)), primary organic aerosols (POA) and black carbon (BC) (identified by colors and markers). **(b and c)** The variations of different aerosol mixing state parameters (identified by colors and markers) at particle size 200 nm **(b)** and 300 nm **(c)**. **(d and e)** The variations of the difference between NF_V and NF_{noBC} (NF_V-NF_{noBC}, blue large circle) and the difference between NF_V and NF_{noBC}+NF_{CBC} (NF_V-(NF_{noBC}+NF_{CBC}), yellow small circle) with the mass concentration of SA at particle size 200 nm **(d)** and 300 nm **(e)** NF_{CBC}**:** Number Fraction of thickly coated black carbon (BC) particles.